Sustainable Energy, Grids and Networks 38 (2024) 101384

Contents lists available at ScienceDirect

Sustainable Energy, Grids and Networks

journal homepage: www.elsevier.com/locate/segan

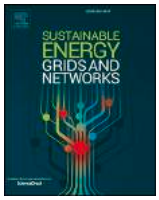

Hierarchical-power-flow-based energy management for alternative/direct current hybrid microgrids

Salar Moradi [a,*], Gibran David Agundis Tinajero [b], Juan C. Vasquez [b], Gaetano Zizzo [a], Josep M. Guerrero [c,d,e], Eleonora Riva Sanseverino [a]

[a] Engineering Department, University of Palermo, Building 9, Palermo, Italy
[b] Department of Energy Technology, Aalborg University, Aalborg 9220, Denmark
[c] Center for Research on Microgrids (CROM), Department of Electronic Engineering, Technical University of Catalonia, Spain
[d] ICREA, Pg. Lluís Companys 23, Barcelona, Spain
[e] CROM, AAU Energy, Aalborg University, Aalborg East 9220, Denmark

ARTICLE INFO

Keywords:
AC/DC hybrid microgrids
Energy management
Hierarchical control
Optimization
Newton-Raphson

ABSTRACT

Modern microgrids are systems comprising both Alternative Current (AC) and Direct Current (DC) subgrids, integrated with Distributed Generations (DGs), storage systems, and Electric Vehicles (EVs) parking facilities. Achieving stable and reliable load flow control amidst varying load, generation, and charging/discharging strategies requires a hierarchical control scheme. This paper proposes an hourly power flow (PF) analysis within an Energy Management System (EMS) for AC/DC Hybrid Microgrids interconnected via an Interlinking Converter (IC) in both grid-connected and islanded modes. The framework operates within a two-level hierarchically controlled platform. Tertiary control at the top level optimizes DGs' reference power for generation and consumption, minimizing power purchase costs and load shedding in grid-connected and islanded modes, respectively. DG converters employ current control mode to share their power references as the primary controller. While no secondary controller is adopted in this scheme, the Battery Energy Storage System (BESS) in islanded mode utilizes P/Q droop control to maintain voltage and frequency in the AC subsystem. Power sharing between AC and DC subgrids through IC is determined by the difference between AC grid frequency and DC link voltage. Integration of controlled converters' buses into PF equations enables solving the unified system using the traditional Newton-Raphson (NR) method. A segment of a real distribution grid planned for installation in Italy under the HYPERRIDE project serves as a case study. Comparison with MATLAB/Simulink results confirms the effectiveness, precision, and convergence speed of the proposed model and control schemes, demonstrating efficient load distribution and voltage/frequency restoration in islanded mode.

1. Introduction

Microgrids have become an efficient and reliable solution integrated into power grids, especially in low voltage ones, due to encompassing widely range of AC and DC systems such as Distributed Generations (DGs), Renewable Energy Sources (RESs), Battery Energy Storage System (BESS), AC/DC cables and loads, among others, that could operate in both grid-connected and islanded modes. Due to an increase in DC loads and penetration of RESs with DC power generation in the last decades, implementing hybrid AC/DC microgrids leads to have the advantages of both AC and DC subgrids simultaneously including a drop in power conversion and more reliable load supply while operating in islanded mode [1]. However, some challenges have emerged for this configuration, particularly related to control context, because of the presence of the coupling of AC and DC subgrids through converters [2–4].

Obviously, power flow (PF) analysis, as the elementary tool in power systems, plays a significant role for other important assessments such as control, protection, design, planning, and energy management, among others. Unlike the conventional power systems, where power flow is characterized using known bus types, in AC/DC hybrid microgrids, particularly in islanded mode, due to the limit and non-robust generation source as a slack bus to keep the voltage and frequency of the network at the rated values, the corresponding buses are not categorized into traditional ones. Additionally, interconnection and power sharing

* Corresponding author.
E-mail address: salar.moradi@community.unipa.it (S. Moradi).

https://doi.org/10.1016/j.segan.2024.101384
Received 15 November 2023; Received in revised form 21 March 2024; Accepted 7 April 2024
Available online 10 April 2024

Nomenclature

Indices and Sets

t	Index for time interval
n,m	Index for bus in AC/DC grids
Ω_{ac}	Set of buses in AC grid
Ω_{dc}	Set of buses in DC grid
T_{out}	Set of hours EVs are out of the parking lot

Parameters

k_{ic}^{p}	Active power droop coefficient for interlinking converter
ω/ω^{*}	Operation and reference frequency [Hz]
$\omega^{\max}/\omega^{\min}$	Upper and lower limit for frequency [Hz]
V_{dc}^{*}	Reference voltage at DC link [V]
$V_{dc}^{\max}/V_{dc}^{\min}$	Upper and lower limit for DC link voltage [V]
c_g	Price of power purchased from the main grid [€]
P_l^{ac}/P_l^{dc}	Active power consumption in AC and DC grids [kW]
Q_l^{ac}	Reactive power consumption in AC grids [kVar]
M	Large positive constant
$P_g^{\max}/Q_g^{\max}$	Upper limit for active and reactive power purchased from the main grid [kW/kVar]
$P_{\max}^{pv}$	Upper limit for active power generated by PV systems [kW]
$P_{ic}^{\max}$	Active power transmission capacity of the IC [kW]
S_{ic}/S_{pv}	Apparent power of the interlinking and the converter connected to PV systems [kVA]
S_s/S_e	Apparent power of the converters connected to BESS and EV parking lot [kVA]
$P_{dis}^{s,\min}/P_{dis}^{s,\max}$	Lower and upper limit for discharging power at BESS in AC and DC grids [kW]
$P_{ch}^{s,\min}/P_{ch}^{s,\max}$	Lower and upper limit for charging power at BESS in AC and DC grids [kW]
$P_{dis}^{e,\min}/P_{dis}^{e,\max}$	Lower and upper limit for discharging power at EV lot in AC and DC grids [kW]
$P_{ch}^{e,\min}/P_{ch}^{e,\max}$	Lower and upper limit for charging power at EV lot in AC and DC grids [kW]
$U_{ac/dc}^{s}(0)$	Initial available energy at BESS in AC and DC grids [kWh]
$U_{ac/dc}^{e}(0)$	Initial available energy at EV's parking lot in AC and DC grids [kWh]
$E_s^{\max}/E_s^{\min}$	Upper and lower limit for stored energy at BESS in AC and DC grids [kWh]
$E_e^{\max}/E_e^{\min}$	Upper and lower limit for stored energy at EV parking lot in AC and DC grids [kWh]
$\boldsymbol{Q}$	Efficiency of the batteries in storage systems and EV parking lots [%]
N	Total number of EVs in each subgrid
D	Average distance of movement each EV traverses a day [Km]
t_l	Time that EVs leave parking lot
λ	Discharge rate of EVs' battery per Km [kW/Km]
G/B	Conductance/susceptance of the admittance matrix in AC grid
g	Conductance matrix in DC grid

Variables

C_T	Total price for importing power from the main grid [€]
P_g	Active power injected from the main grid [kW]
Q_g	Reactive power injected from the main grid [kVar]
P_{ac}^{pv}/Q_{ev}^{dis}	Active and reactive power generated by PV in AC grid [kW/kVar]
$P_{dis}^{s,ac}/P_{ch}^{s,ac}$	Charging/discharging active power at BESS in AC grid [kW]
$P_{dis}^{e,ac}/P_{ch}^{e,ac}$	Charging/discharge active power at EV parking lot in AC grid [kW]
Q_{ac}^{s}/Q_{ac}^{ev}	Reactive power generated by BESS and EV parking lot in AC grid [kVar]
P_{ic}/Q_{ic}	Active and reactive power transferred through the IC [kW/kVar]
P_{dc}^{pv}	Active power generated by PV in DC grid [kW]
$P_{dis}^{s,dc}/P_{ch}^{s,dc}$	Charging/discharging active power at BESS in DC grid [kW]
$P_{dis}^{e,dc}/P_{ch}^{e,dc}$	Charging/discharge active power at EV parking lot in DC grid [kW]
$I_{dis}^{s,ac}/I_{ch}^{s,ac}$	Binary variable showing charging/discharging status of BESS in AC grid
$I_{dis}^{e,ac}/I_{ch}^{e,ac}$	Binary variable showing charging/discharging status at EV parking lot in AC grid
$I_{dis}^{s,dc}/I_{ch}^{s,dc}$	Binary variable showing charging/discharging status of BESS in DC grid
$I_{dis}^{e,dc}/I_{ch}^{e,dc}$	Binary variable showing charging/discharging status at EV parking lot in DC grid
I_{ic}	Binary variable showing the direction of power transferred by IC
$E_{ac/dc}^{s}/E_{ac/dc}^{e}$	Energy available at BESS and EV parking lot in both AC/DC grids [kWh]
L_T^{sh}	Total load shedded
γ^{ac}/γ^{dc}	Rate of load shedding in AC and DC grids
$P_{l,i}^{ac}/Q_{l,i}^{ac}$	Active/reactive power consumption in islanded mode in AC grid [kW/kVar]
$P_{l,i}^{dc}$	Active power consumption in islanded mode in DC grid [kW]
P_n^{ac}/Q_n^{ac}	Active/reactive power injected to the nth bus in AC grid [kW/kVar]
P_n^{dc}	Active power injected to the nth bus in DC grid [kW]
$\lvert V_n\rvert/\lvert V_m\rvert$	Voltage magnitude of the nth/mth bus [p.u.]
δ_n/δ_m	Phase angle of the nth/mth bus [radians]

between AC and DC subgrids needs to adopt a proper control scheme, preventing buses to fall into PQ or PV buses [5–7]. Therefore, a comprehensive control framework is integrated to power flow analysis in coupled AC/DC microgrids. Since solving control-integrated PF in power management prospective, it is crucial to implement hierarchical control scheme, and to adopt a proper power flow calculation technique. Therefore, literature below discusses different inner control layers as primary and secondary controllers, top layer playing the role of power management, and PF analysis techniques respectively, in various AC/DC hybrid networks topologies.

Power flow analysis in controlled hybrid microgrids has increased researchers' interests in the last decade. They mainly have focused on the islanded operation mode. To PF assessment in AC/DC hybrid microgrids, authors in [8–16] have tried to define new controlled buses for both AC and DC buses in islanded mode, applying well-known droop control. In [8], authors integrated a two-level, primary and secondary, well-known drooped-based control schemes into traditional Newton-Raphson (NR) power mismatch formulations for islanded AC/DC microgrid to manage power sharing among DGs and restore AC/DC voltages and frequency at point of common coupling (PCC) bus; in addition, a voltage-frequency droop controller is characterized for IC to control power sharing between both subgrids. The same droop based primary controller has been suggested in [9–11] for DG's converters and IC in PF analysis, where [9] tries to evaluate different hybrid microgrid structures, where the model is also applicable for grid-connected mode, and [10] implements the addressed controlled power flow analysis for

Table I
A comparison between the existing literature and the proposed model.

Ref.	Network type	Operating mode	Control scheme			Source/Load contribution			PF calculation	Daily load flow
			primary	secondary	tertiary	RES	BESS	EV		
[6]	AC	islanded	✓	✓	✓	✓	✓			✓
[8]	AC/DC	islanded	✓	✓					unified	
[9]	AC/DC	Islanded/grid-connected	✓						unified	
[10]	AC/DC	islanded	✓						unified	
[11]	AC/DC	islanded	✓						sequential	
[12]	AC	islanded	✓							
[13]	AC/DC	islanded	✓			✓	✓	✓	sequential	
[14]	AC/DC	islanded	✓			✓	✓		unified	
[15]	AC	islanded	✓		✓					
[18]	AC/DC	Islanded/grid-connected	✓		✓	✓	✓			
[19]	AC	grid-connected			✓	✓	✓			✓
[20]	AC/DC	islanded			✓	✓	✓			✓
[21]	AC/DC	grid-connected	✓		✓	✓	✓			✓
[22]	AC/DC	islanded	✓	✓		✓				
[23]	AC/DC	grid-connected							sequential	
[24]	AC/DC	grid-connected							unified	
[25]	AC/DC	Islanded/grid-connected	✓						unified	
[26]	AC/DC	Islanded/grid-connected	✓							
This paper	AC/DC	Islanded/grid-connected	✓		✓	✓	✓	✓	unified	✓

multiple AC-DC hybrid structures. Different droop characteristics, based on the output impedance of DGs, have been included in PF mismatch equations [12], where change the Jacobian and variable matrices. In [13], popular P-ω/Q-V droops in AC grid and P-V droop in DC one are adopted in a backward-forward sweep (BFS) algorithm for calculating load flow sequentially. This approach is developed for decomposed AC and DC subgrids which are coupled using normalized V-ω droop [3,8] for IC. Unlike works above, [14] consider Renewable Energy Sources (RESs) and storage systems in AC and DC subgrids as well. The most significant point in this work is to control charging/discharging status of storage systems in AC and DC grids through frequency and DC terminal voltage respectively. Droop characteristics and voltage reference of DG units in [15] are extracted from Optimal Power Flow (OPF), which play as reference roles for voltage source control converters in islanded AC microgrid. A new idea is developed in [16] to control power exchange between AC and DC subgrids in grid-connected mode, where a modified unified interphase power controller is implemented, including one line power converter and one bus power converter regulating dc link voltage.

Regarding top control level, including tertiary control in the EMS framework, some authors have addressed power management [17–22]. Ref. [17] provides a comprehensive review of power management strategies in AC/DC hybrid microgrids including different system structures, different operation modes in both steady-state and transient conditions. A hierarchical energy management for storage-photovoltaic based hybrid microgrids is applied in [18], where it comprises a centralized supervisory system to decide the control scheme and power reference sets, for both islanded and grid-connected modes, to the converters' local controllers. However, [19] and [20] adopted energy management only in tertiary level, which calculates hourly optimal charging/discharging strategies for storage systems [19], and a stochastic optimal load flow is adopted in [20] to measure power sharing among DGs and RESs considering uncertainty of variables. Authors in [21] and [22] suggested hierarchically power management, where it is divided into two system-level and devise-level perspectives [21], at which the former is implemented by mixed-integer optimization program, then power reference control mode is applied to converters as the latter level. Meanwhile, [22] includes only autonomous primary and centralized secondary controllers. In addition, small-signal stability analysis is conducted to investigate the influence of the communication delays on the system stability.

In general, power flow calculations in AC/DC hybrid grids are solved using two methodologies: sequential and unified. In the former [11,13], and [25], parameters in one system (usually in DC one) are estimated, then power flow for another one is solved, and finally estimated parameters are updated till convergence is reached. However, in the latter approach [8–10,14], AC and DC power flow equations are solved simultaneously. Since convergence problem in sequential method might rise [23], and to have better convergence characteristics in unified one [24], this paper solves power flow equations as a unified system.

Almost all the works mentioned above have only considered islanded mode. Modern microgrids consist of RESs, storage systems, and modern loads such as Electrical Vehicles (EVs), where they can operate in grid-tied or islanded modes. On the one hand, the steady-state dynamics in each operation mode require specific decision making taken by the top control (tertiary level in this paper) and might change the control scheme of some sources. On the other hand, the intermittent dynamics of RESs and EVs during a day cause changes in load supply, charging/discharging states for BESS and EV parking lots. Therefore, a top control layer is needed for daily power flow analysis in both operating modes. A few works have studied controlled-power-flow analysis in both grid-connected and islanded operating modes [25], and [26]. These articles do not address the research gaps mentioned above, as authors propose constant power DGs in hybrid microgrids, incorporating them into power flow formulation using droop control.

This paper aims to present a comprehensive hierarchically controlled power flow analysis for AC/DC hybrid microgrids in both grid-connected and islanded operating modes, considering the challenges above. For each operation mode, a centralized tertiary controller, as an energy management system, runs an optimization problem to calculate power generation, charging/discharging references for PVs, BESSs, and EVs. This could be mentioned as a drawback of the proposed control scheme, as a single point centralized unit leads to a decrease in reliability, and its failure results in a loss of power-sharing control for the entire system. Furthermore, the paper studies the case of a real grid, as a part of a project named HYPERRIDE, that is going to be installed as a part of the Italian distribution power system with fully embedded RESs and flexible sources like BESS and Electrical Vehicles (EVs) stations in both AC and DC subgrids, whereas works discussed in the literature study experimental test systems, and such a configuration with EV contribution has not been studied. Another novelty is that the proposed model incorporates a flexible primary controller for the converter integrated with BESS installed on the AC side, depending on the operating mode. In grid-connected mode, current reference control mode is adopted for DGs in both AC and DC grids, since the main grid is responsible to keep voltage and frequency at PCC bus. Interlinking converter uses a frequency-voltage droop to calculate power reference for its corresponding AC/DC buses, and to exchange power between both subgrids, keeping DC link voltage close to its nominal value. In

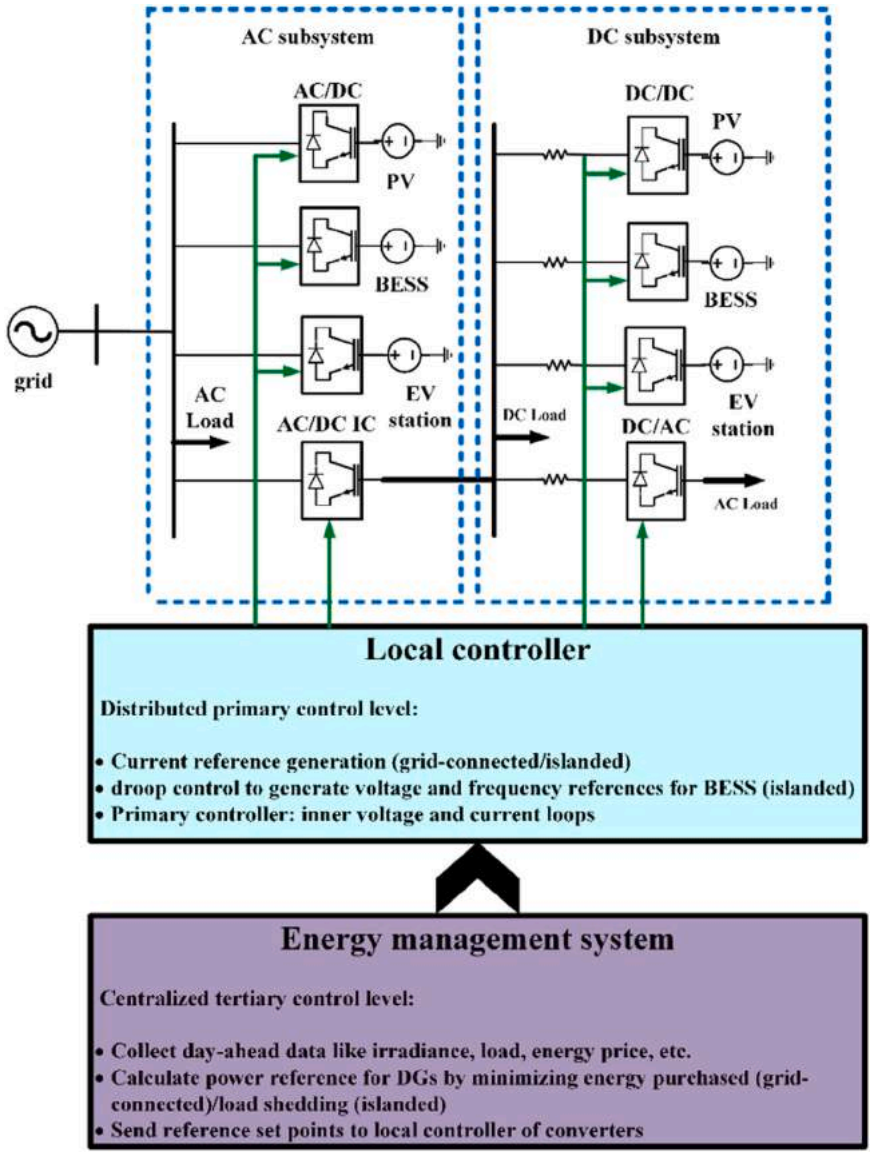

Fig. 1. General Framework of the proposed hierarchically controlled optimal power flow.

islanded mode, all converters remain with the same control mode, but the one connected to BESS in AC subgrid. Note that in previous studies, authors almost propose at least one voltage source converter (VSC) in AC and DC grids, making control schemes more complicated; however, in this paper, the VSC connected to BESS in AC side generates voltage and frequency references at PCC bus using V-f droop control. This platform leads to have a simple and fast control scheme, while no need to change other converters' control mode. In addition, it is not necessary to adopt voltage and frequency restoration controllers as secondary one.

To have power reference for buses as schedule set points, power flow equations for both AC and DC subgrids are solved in a unified system using NR algorithm, which results in sufficiently fast convergence, as shown in the case study section. Finally, the results for mathematical model are validated by comparing against the professional simulation software MATLAB/ Simulink, approving the effectiveness and precision of the proposed model and control schemes.

This article focuses on studying power flow in hybrid microgrids, exclusively addressing steady-state operation for both grid-connected and islanded modes. Consequently, the transient period is not considered in this paper. It is important to note that in transient studies, secondary voltage/frequency regulation becomes essential for rapid voltage restoration. As a result, the proposed model may not be deemed feasible or practical in transient states. Based on the identified research gaps in the literature and the novelty of this study, Table I represents comparison between existing literature and the proposed model.

The rest of the paper is organized as follows. Section II explains the procedure of the proposed model and hybrid system in detail. In section III, the control schemes for DGs' converter in AC and DC subgrids are shown, and the interlinking converter controller and its integration in power flow model are presented. The optimization and power flow problems for 24-hour period are modeled in Section IV. Section V contains the case study analysis and the related result discussion. Finally, Section VI reports the conclusion of the paper.

2. Hierarchically controlled optimal power flow in AC/DC hybrid microgrids

In this section the proposed model and hierarchical control scheme is presented in detail. First, it is vital to recognize the proposed AC/DC hybrid microgrid and its elements. Therefore, Fig. 1 shows an outlook of the system under study including electrical component, and controllers. In this hybrid structure, AC subgrid is connected to the main grid at PCC

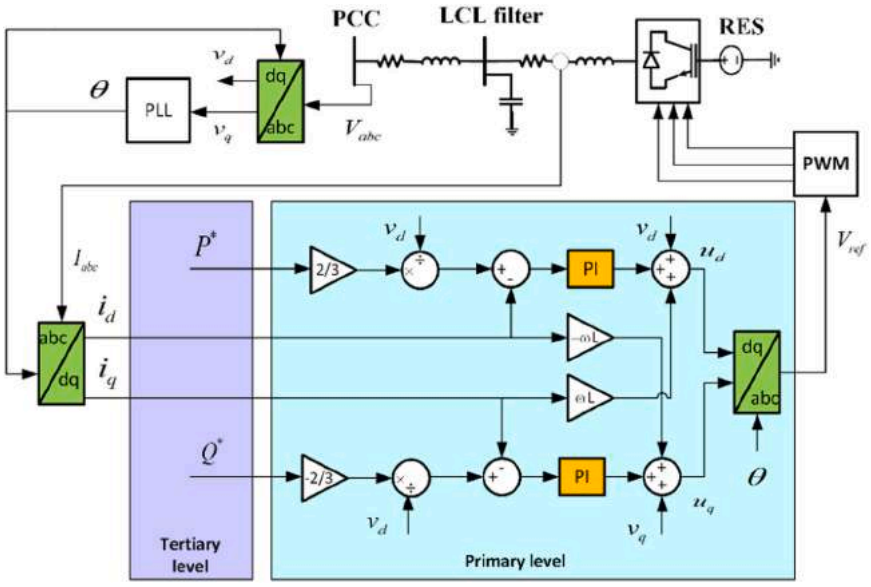

Fig. 2. Hierarchical control scheme for RESs in AC subgrid.

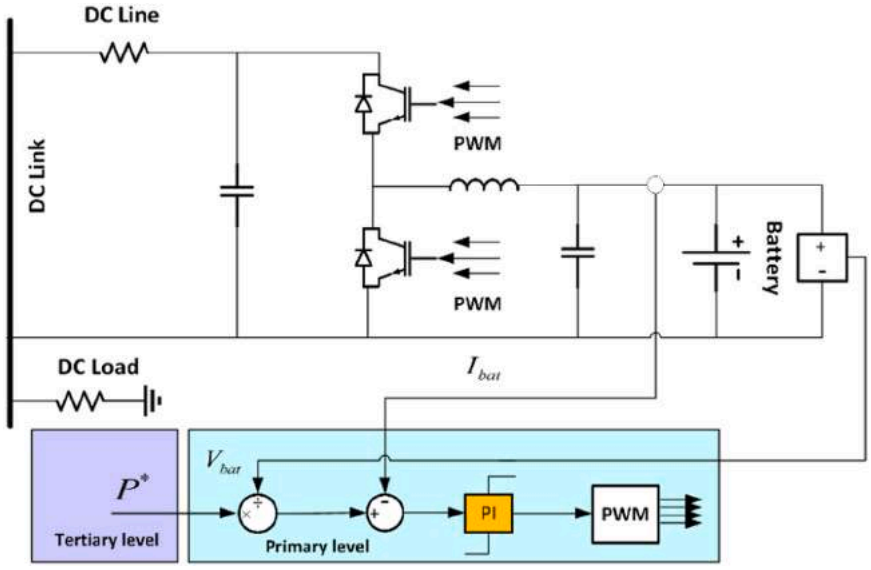

Fig. 3. Hierarchical control scheme for BESS ad EV station in DC subgrid.

bus. AC and DC subgrids are connected through a bidirectional AC/DC IC. In each subsystem, there is a PV-Storage system and an EV charging/discharging station which are connected to the corresponding AC/DC buses by proper converters. Local AC and DC loads are located at PCC and DC link respectively, another AC load is supplied from DC subgrid through a DC/AC inverter, as well. In addition, Fig. 1 depicts the proposed hierarchically controlled optimal power flow, which is explained in the following subsections.

2.1. Tertiary control

In the present work, tertiary control plays the role of the energy management system and is responsible for determining the hourly optimal power shares for the main grid (in grid-connected mode), PV systems, BESSs, and EV stations. The system also determines charging/discharging of storage systems and from EV stations, as well as the power exchange between AC and DC subgrids through IC, unlike the literature where changes in loads and RESs' output power over time are not addressed [6], or where only power exchange between microgrid and the main grid, along with charging/discharging for storage systems are considered [19–21]. Tertiary controller collects day-ahead data for AC and DC loads, output power for PV systems, and energy price, and characterizes an optimization problem, where the objective function is to minimize total cost for purchasing energy from the main grid in grid-connected mode, and load shedding in islanded mod. The references set given by the tertiary control are delivered to the converters local controllers using communication network, considered as scheduled power, as well, for power flow mismatch equations. Tertiary control's mathematical model and power flow equations are described in detail in section IV.

2.2. Primary control

Power set points calculated in tertiary control level are delivered to the converter's local controller, including primary control level. As it is mentioned in the introduction section, in the proposed control scheme,

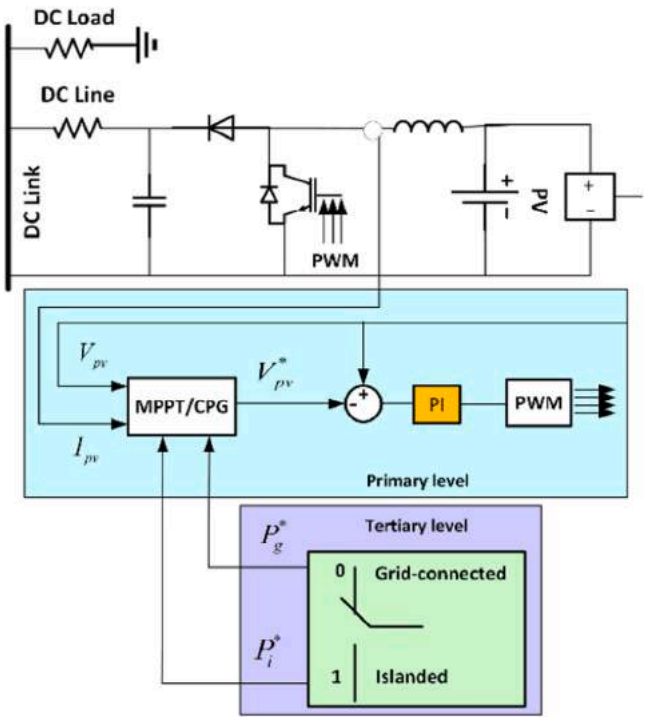

Fig. 4. Hierarchical control scheme for DC-side PV system in grid-connected and islanded modes.

there is no need to have voltage and frequency restoration at the PCC bus in the AC subgrid in both grid-connected and islanded modes as a secondary control level. In addition, since the interlinking converter controller uses a frequency/DC-voltage droop to supply the missing power to both subgrids, the DC link voltage is regulated autonomously and there is no need to control the DC bus voltage.

In grid-connected mode, voltage and frequency at PCC bus are regulated by the main grid. In this case, all RESs' converters, in both AC and DC subgrids, follow current control mode to generate reference powers [27]. Therefore, current reference generation, and inner voltage and current loops act as the primary controller. Note that, RESs generate power references, while the main grid supplies active and reactive powers close to its references (from the tertiary controller) to compensate power losses of the converters' filter and dc line resistances.

In islanded mode, all converters remain on the current control mode but that one is connected to the battery storage system in the AC subgrid being responsible to restore voltage and frequency at PCC through frequency/active power and voltage/reactive power droops as the primary controller [27]. BESS in AC subgrid projects like the main grid in grid-connected mode, keeping voltage and frequency respect to charging/discharging power reference values. For example, assuming a discharge operating mode, BESS tries to supply powers a little bit more than references to offset power losses, regulating voltage and frequency.

3. Hybrid microgrid control scheme

This section presents control schemes for RESs converters and IC converters for AC and DC subgrids in both grid-connected and islanded operation modes. The following subsections depict these control specifications for AC and DC grids.

3.1. Grid-connected mode

In grid-connected operating mode, since the main grid keeps the AC subgrid voltage and frequency at their reference values and compensates the power losses of the lines and filters, all converters in both AC and DC subgrids conduct current reference control mode to generate a fixed

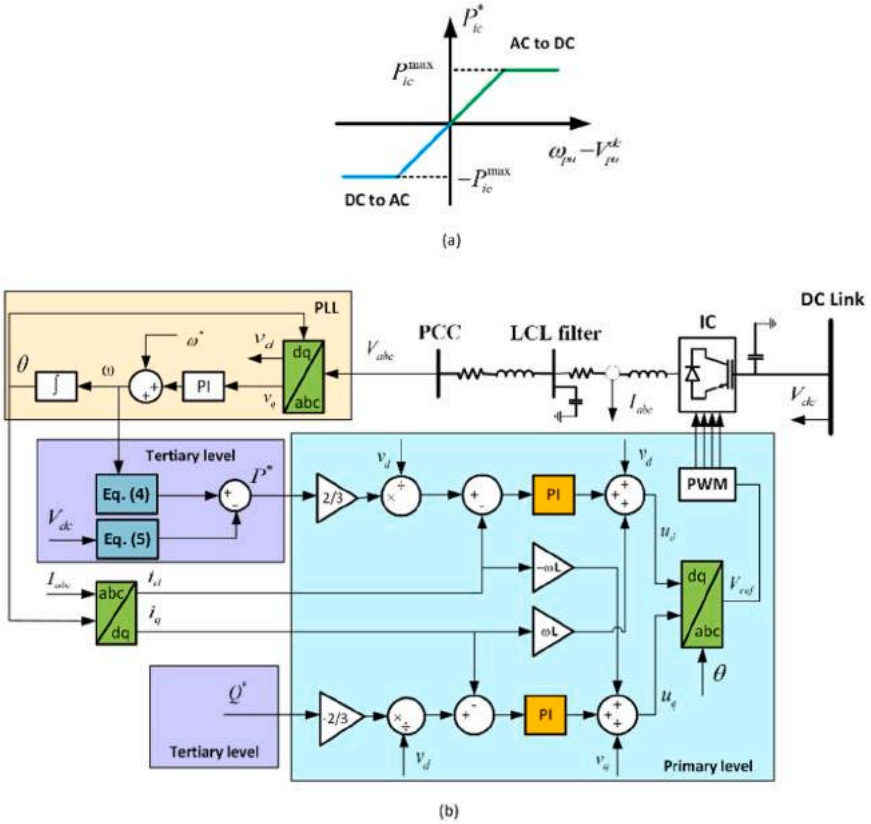

Fig. 5. (a): IC droop control for active power sharing, (b): Hierarchical control scheme for IC.

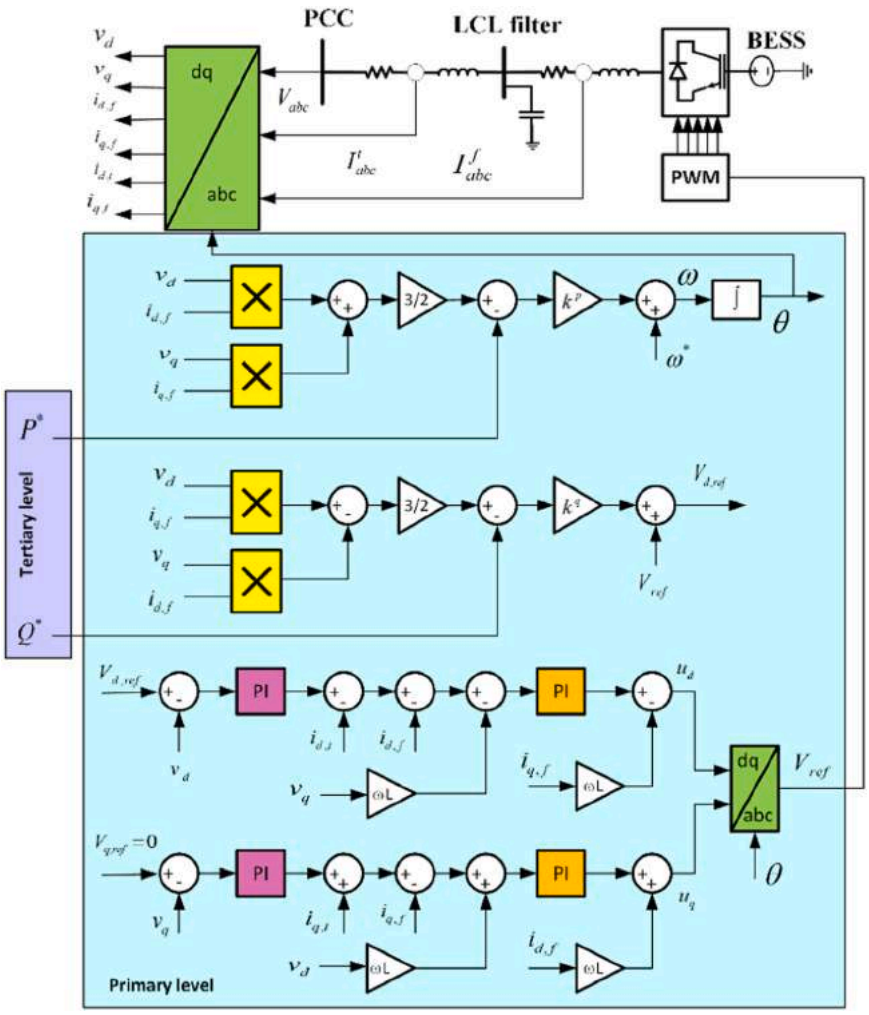

Fig. 6. Hierarchical control scheme for AC-side BESS in islanded mode.

power calculated in the tertiary control level as optimal power sharing. Hierarchical-based current control schemes for RESs in both AC and DC subgrids are illustrated in Figs. 2 and 3, respectively. For RESs' converters in AC subgrid (Fig. 2), the three-phase inductor currents and voltages at the PCC are measured to be transformed into synchronous d-q frame using Park's transformation, and its angular position is generated and controlled through Phase Locked Loop (PLL) so that v_q component matches to zero [21,27,28]. Dynamic equations to calculate current references in d-q frame are as follows:

$$i_d^* = \frac{2P^*}{3v_d} \tag{1}$$

$$i_q^* = \frac{2Q^*}{3v_d} \tag{2}$$

where, P^* and Q^* are active and reactive power references, coming from the EMS and delivered to the primary local controller of the converters. Using these power references, Eqs. (1) and (2) calculate current references in d-q frame. Finally, the inner current loop generates the voltage reference required for Pulse Width Modulation (PWM).

In DC subgrid, however, battery storage system and electrical vehicles station are connected to the DC link through a bidirectional buck-boost converter and a line (represented as a resistance in Fig. 3). Current control principle for DC/DC converters follows the same as that for AC/DC converters in the AC subgrid. P^* from the tertiary controller is transferred to the local controller. Then, using measured dc voltage of the battery, current reference is produced, followed by inner current loop as the primary control level to generate voltage reference. This voltage generates PWM signals, applying to buck-boost converters.

For a DC/DC boost converter connected to PV system, Fig. 4 depicts the control block diagram for both grid-connected and islanded operation modes since they follow almost similar structure. In islanded mode, microgrid needs to use maximum output power of PV system to implement minimum load shedding. Therefore, in optimization process (tertiary level), a fixed PV output power (P_i^*) is taken into account for each hour depending on irradiance and goes to perturb and observe maximum power point tracking (P&O-MPPT) algorithm. However, in grid-connected mode, optimization program might choose PV output power lower than maximum available power. By this case, boost converter is going to generate P_g^* using P&O constant power generation (P&O-CPG), see Fig. 4. In this algorithm, the PV output voltage is continuously perturbed away from the maximum power point in the CPG operation mode in order to match the PV output power according to the set point. Readers may refer to [29,30] to have a deeper understanding of CPG control mode in PV system. In both cases, finally, an inner voltage loop is conducted to generate PWM signals.

The Interlinking Converter (IC) is the most important component in hybrid grids to share power between both AC and DC subgrids. A properly controlled IC leads to a stable and robust power exchange between AC and DC subgrids. According to the power references characterized by the tertiary controller, if total output power of the RESs in DC grid is not sufficient to supply DC local load, IC transfer power shortage

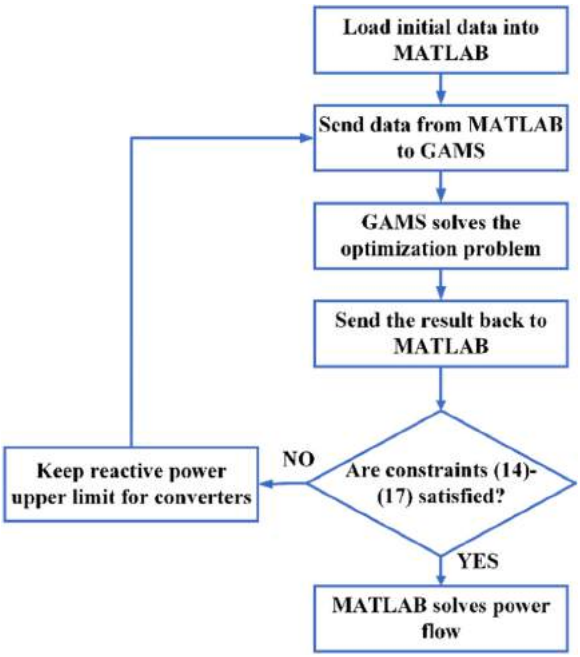

Fig. 7. The interlinking process between MATLAB and GAMS.

from AC to DC grid to keep DC link voltage close to the nominal value, and vice versa delivers surplus DC active power to AC grid to keep frequency at PCC. Therefore, in this paper a well-known $P/\omega_{pu} - V_{pu}^{dc}$ droop control is conducted and shown in Fig. 5(a), meaning IC shares active power based on the difference between frequency at PCC and DC link voltage [3, 8, and 27]. This active power is purposed as scheduled active power in mismatch equations in NR algorithm, and calculated as follows:

$$P^{*} = \frac{\omega_{pu} - V_{pu}^{dc}}{k_{ic}^{p}} \tag{3}$$

Where, ω_{pu} and V_{pu}^{dc} are normalized (per unit) measured frequency at PCC and dc link voltage, respectively, to be comparable, and calculated as:

$$\omega_{pu} = \frac{\omega - \omega^{*}}{0.5(\omega^{\max} - \omega^{\min})} \tag{4}$$

$$V_{pu}^{dc} = \frac{V_{dc} - V_{dc}^{*}}{0.5\left(V_{dc}^{\max} - V_{dc}^{\min}\right)} \tag{5}$$

According to Eq. 5(a) and Eq. (3), whenever per unit frequency is greater than the per unit DC link voltage, active power is delivered to the DC grid to compensate deficient available power there, and inversely, lower frequency at PCC due to power shortage makes IC to transfer

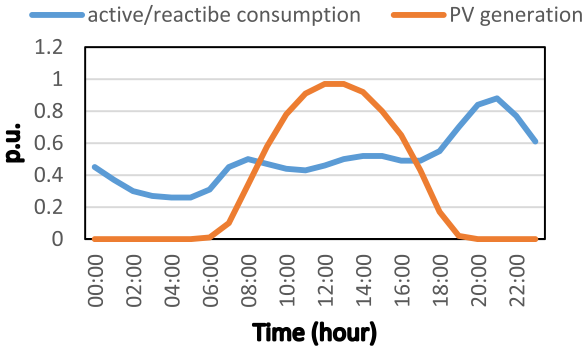

Fig. 9. Hourly load demand and PV generation in p.u.

Table II
Capacity of the resources and load demand in AC and DC subgrids.

subgrid	PV [kW]	BESS [kWh]	EV station [kWh]	Load [kW/kVar]
AC	10	50	50	30/10
DC	5	50	50	Load #1 → 20 Load #2 → 25

Table III
Energy price in Italian case study.

weekdays	Time (hour)	Price (€/kWh)
Monday-Friday	23:00–7:00	0.4121
Monday-Friday	7:00–8:00	0.4955
Monday-Friday	8:00–19:00	0.4417
Monday-Friday	19:00–23:00	0.4955

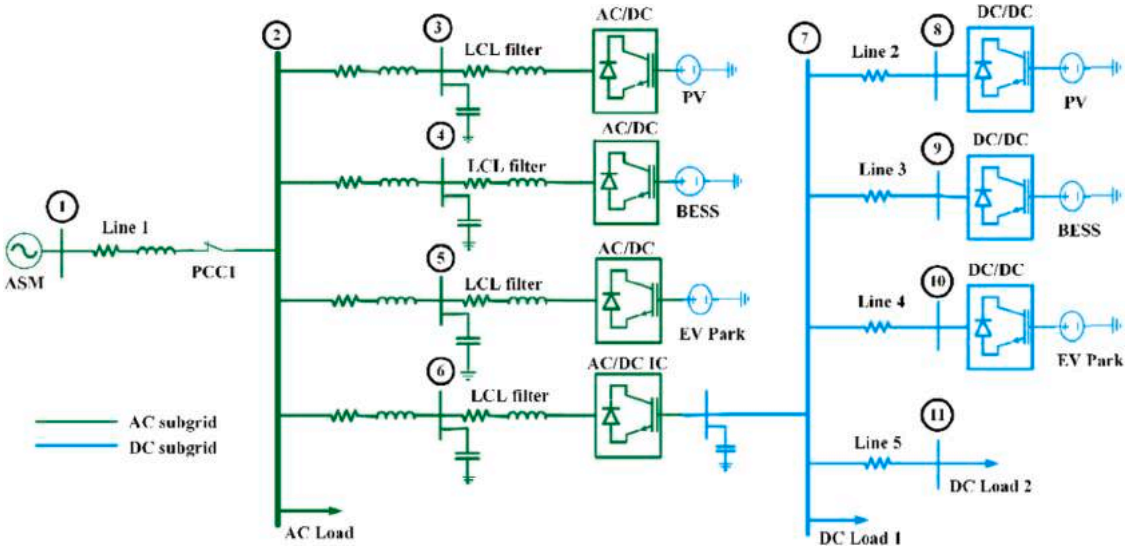

Fig. 8. Terni AC/DC hybrid microgrid: Italian Pilot.

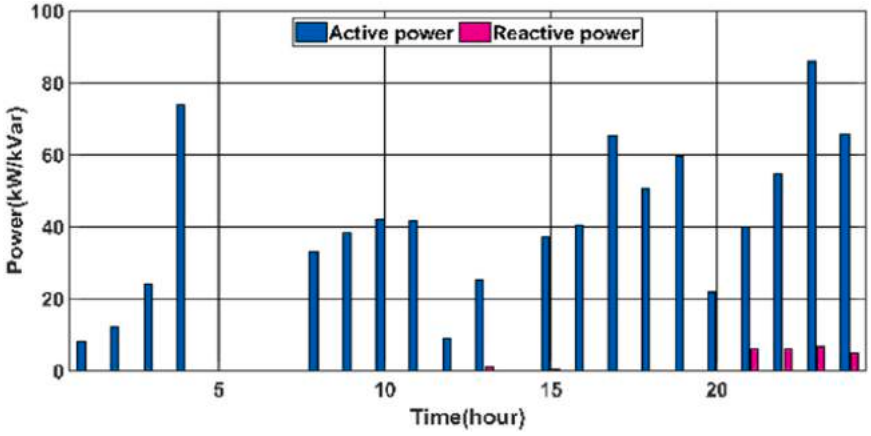

Fig. 10. Hourly power purchased from the main grid.

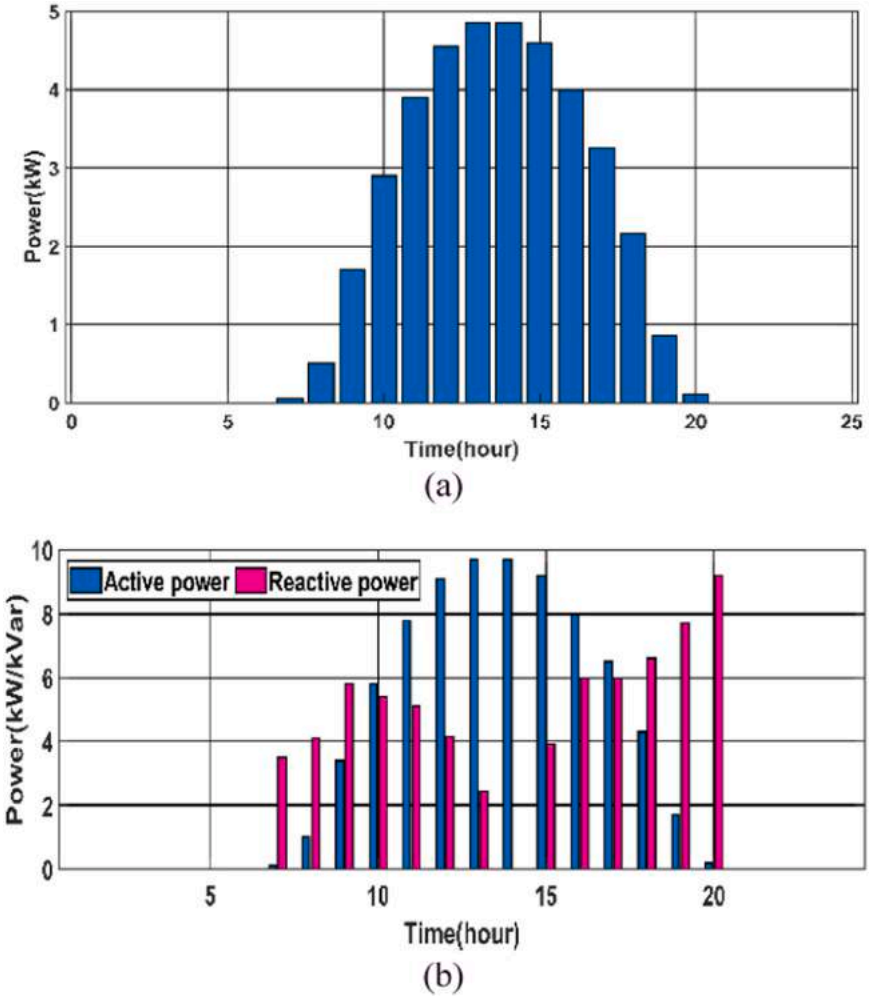

Fig. 11. Hourly power generated by PV system: (a) DC grid, (b) AC grid.

surplus DC active power from DC side to AC one. Note that the reference set-point for the reactive power is calculated in the optimization process, done by the tertiary level controller. It is worth to mention that, only if there is power sharing from DC to AC side, IC may deliver reactive power to AC grid [27]. Fig. 5(b) illustrates the hierarchical control block diagram that is the same as that for RESs' controllers in AC side (Fig. 2), but active power reference is coming from Eq. (3).

3.2. Islanded mode

As it is discussed in the introduction section, this paper proposes that, in the islanded mode, the control scheme of all converters remain the same as in grid-connected mode with the exception of that connected to BESS in AC subgrid. Since PV system and EVs are not able to generate energy for a 24-hours day, BESS need to change its control mode to voltage control mode [31] as depicted in Fig. 6. Active and reactive

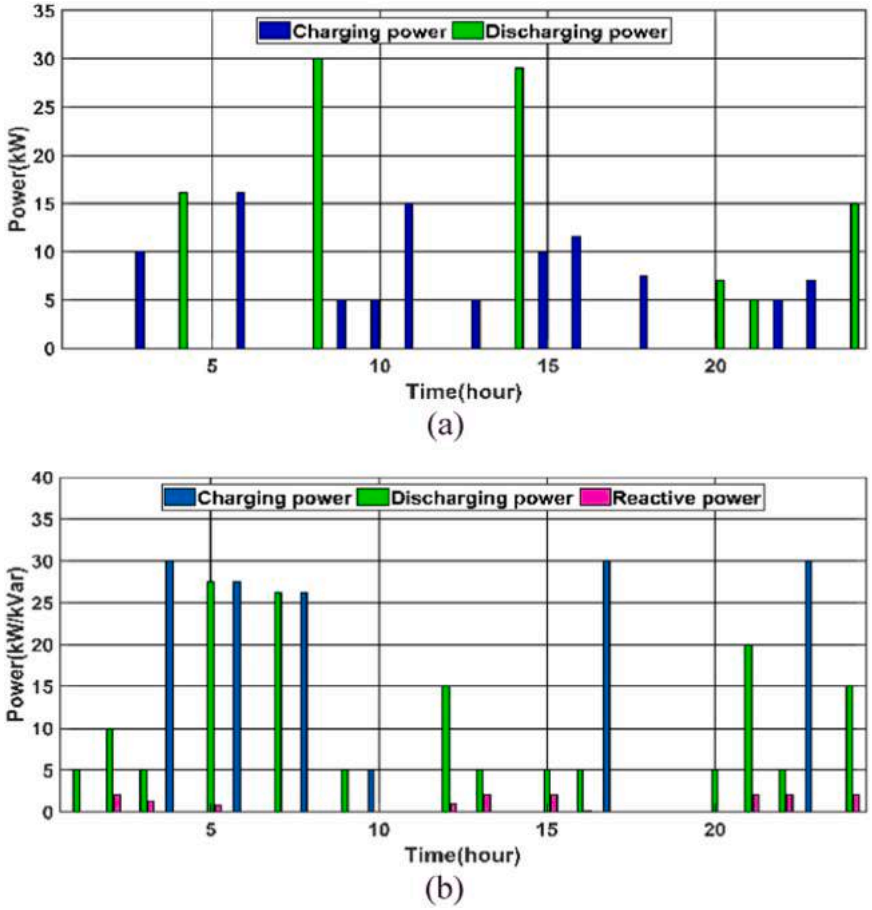

Fig. 12. Hourly charging/discharging power at BESS: (a) DC grid, (b) AC grid.

power are calculated and compared to references values coming from the upper level, which could be positive or negative dependent on charging/discharging operation modes. Then, a droop-based primary controller is applied to generate reference voltage and angular frequency. Then, using these values, inner voltage and current loops generate PWM pulses for the converter. In fact, this control scheme aims to keep voltage and frequency at PCC, while trying to follow power references. In other word, when storage system operates in discharging state, it may generate active and reactive power a little more than reference values and consumes a little lower than reference active power in charging mode. In fact, this difference is due to power losses compensation by storage system to hold nominal voltage and frequency at PCC.

4. Tertiary level and power flow formulation

In this section, the tertiary control level, that is an optimization program, and the Newton-Raphson power flow equations are mathematically modeled for both AC and DC subgrids in grid-connected and islanded operating modes. Although the proposed model is formulated in general for any AC/DC power grid outline, readers may refer to Fig. 1, as it presents the same system used in the case study (single-line diagram is shown in section V), to better understand the concept of the mathematic model. The two first following subsections describe and formulate the daily optimal load sharing for both operation modes, then unified AC/DC NR power flow equations are solved integrating scheduled powers from the optimization, and the control scheme for the interlinking converter.

4.1. Grid-connected mode

In grid-tied operation mode, the aim of tertiary control level, which plays an EMS, is to determine power generation references for RESs along with charging/discharging states for batteries of BESSs and EVs each hour, meanwhile minimizing the total cost of the power purchasing from the main grid. In this scenario, all RESs follow current control mode to generate the reference powers, and PV system switches to constant power generation mode (position "0" for the switch in Fig. 4) that implies it might generate power lower than maximum power each hour. So, if all RESs in both subgrids follow their power set-points, the main grid also deliver power to the microgrid as much as calculated from the optimization program. Therefore, the objective function is:

$$C_T = \sum_{t=1}^{24} c_g(t) * \left(P_g(t) + Q_g(t)\right) \tag{6}$$

From (6), it is worth noting that, although energy price is often based on active power, utilities sometimes charge customers for a poor power factor. In addition, PV and storage system on the AC subsystem may inject reactive power into the microgrid. Therefore, importing reactive power from the main grid is considered as a penalty in this article.

Constraints are categorized into two types including load sharing-related and battery-oriented ones. Equations and inequalities (7)-(17)

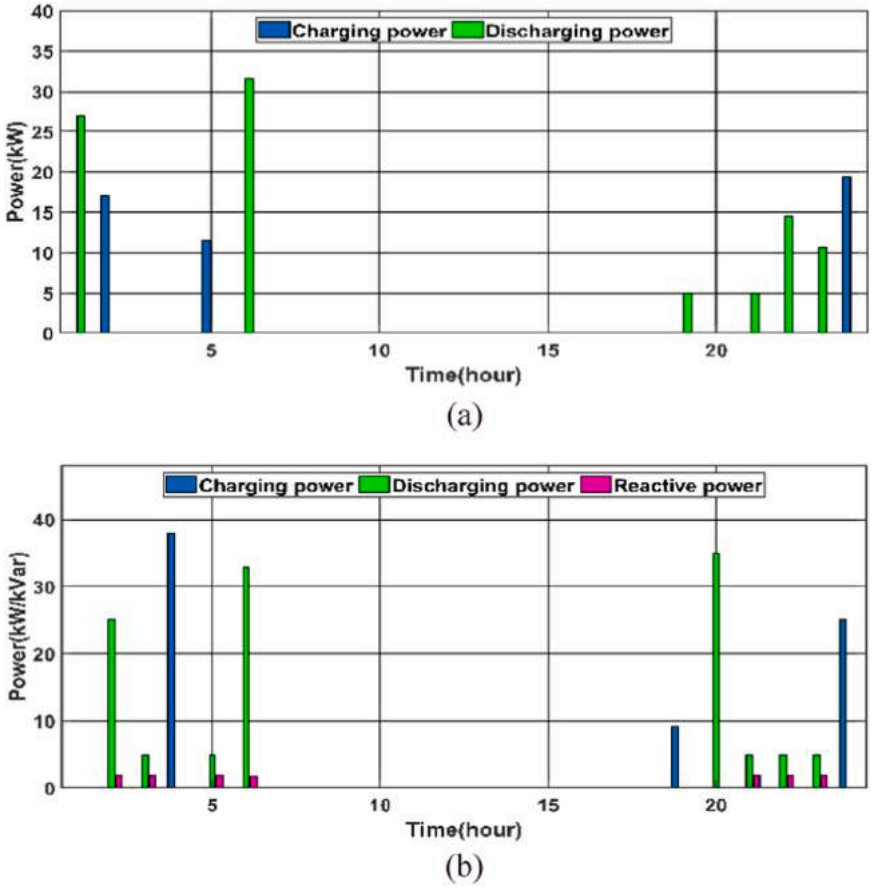

Fig. 13. Hourly charging/discharging power at EV parking lot: (a) DC grid, (b) AC grid.

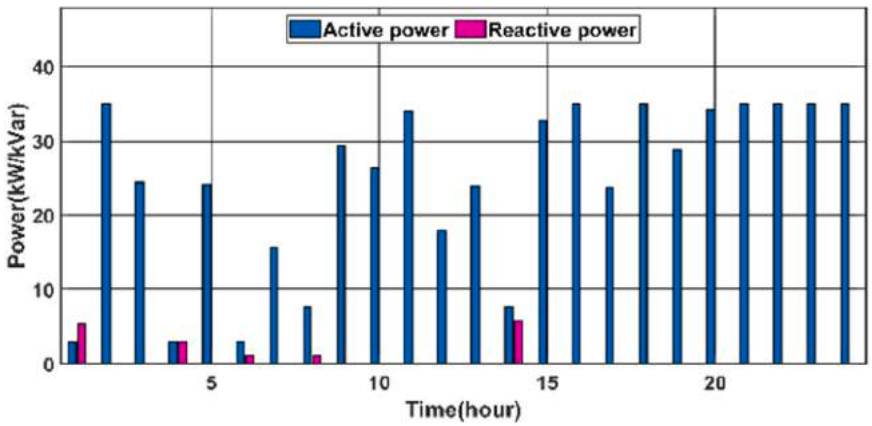

Fig. 14. Hourly power transferred through interlinking converter.

represent the first category. Eqs. (7)-(9) represent active and reactive power balance. For active power, there are two sets of power balance equations meaning Eq. (7) and Eq. (8) depending on the direction IC transmit active power. In the first set, it is from AC to DC implying IC is a load for AC subgrid, meanwhile playing a role as a source for DC subgrid. Unlike the first equations set, in the second set, characterized in (8), IC is a load for DC side, while a source for AC one. To mathematically model this aspect in optimization process, a very large number M and an integer variable I_{ic} for the direction of active power sharing for IC are defined. If program makes IC to send active power from AC to DC, I_{ic} would be 1, equations in (7) must be zero and those in (8) are free. Inversely, when optimization prefers to transmit active power from DC to AC side, I_{ic} would be 0, equations in (8) are chosen, and those in (7) are relax.

$$\begin{cases} P_{ac}^{pv}(t)+P_g(t)+P_{dis}^{s,ac}(t)+P_{dis}^{e,ac}(t)-P_{ch}^{s,ac}(t)-P_{ch}^{e,ac}(t)-P_l^{ac}(t)-P_{ic}(t)\geq -M\left(1-I_{ic}(t)\right) \\ P_{ac}^{pv}(t)+P_g(t)+P_{dis}^{s,ac}(t)+P_{dis}^{e,ac}(t)-P_{ch}^{s,ac}(t)-P_{ch}^{e,ac}(t)-P_l^{ac}(t)-P_{ic}(t)\leq M\left(1-I_{ic}(t)\right) \\ P_{dc}^{pv}(t)+P_{dis}^{s,dc}(t)+P_{dis}^{e,dc}(t)+P_{ic}(t)-P_{ch}^{s,dc}(t)-P_{ch}^{e,dc}(t)-P_l^{dc}(t)\geq -M\left(1-I_{ic}(t)\right) \\ P_{dc}^{pv}(t)+P_{dis}^{s,dc}(t)+P_{dis}^{e,dc}(t)+P_{ic}(t)-P_{ch}^{s,dc}(t)-P_{ch}^{e,dc}(t)-P_l^{dc}(t)\leq M\left(1-I_{ic}(t)\right) \end{cases} \forall t \tag{7}$$

$$\begin{cases} P_{ac}^{pv}(t)+P_g(t)+P_{dis}^{s,ac}(t)+P_{dis}^{e,ac}(t)+P_{ic}(t)-P_{ch}^{s,ac}(t)-P_{ch}^{e,ac}(t)-P_l^{ac}(t)\geq -M.I_{ic}(t) \\ P_{ac}^{pv}(t)+P_g(t)+P_{dis}^{s,ac}(t)+P_{dis}^{e,ac}(t)+P_{ic}(t)-P_{ch}^{s,ac}(t)-P_{ch}^{e,ac}(t)-P_l^{ac}(t)\leq M.I_{ic}(t) \\ P_{dc}^{pv}(t)+P_{dis}^{s,dc}(t)+P_{dis}^{e,dc}(t)-P_{ic}(t)-P_{ch}^{s,dc}(t)-P_{ch}^{e,dc}(t)-P_l^{dc}(t)\geq -M.I_{ic}(t) \\ P_{dc}^{pv}(t)+P_{dis}^{s,dc}(t)+P_{dis}^{e,dc}(t)-P_{ic}(t)-P_{ch}^{s,dc}(t)-P_{ch}^{e,dc}(t)-P_l^{dc}(t)\leq M.I_{ic}(t) \end{cases} \forall t \tag{8}$$

$$Q_{ac}^{pv}(t)+Q_g(t)+Q_{ac}^{s}(t)+Q_{ac}^{ev}(t)+Q_{ic}(t)=Q_l^{ac}(t) \tag{9}$$

$$P_g(t)\leq P_g^{\max}\forall t \tag{10}$$

$$P_{ac/dc}^{pv}(t)\leq P_{\max}^{pv}\ \forall t \tag{11}$$

$$P_{ic}(t)\leq P_{ic}^{\max}\forall t \tag{12}$$

$$Q_g(t)\leq Q_g^{\max}\forall t \tag{13}$$

$$Q_{ac}^{pv}(t)\leq \sqrt{{S_{pv}}^2-{P_{ac}^{pv}(t)}^2}\forall t \tag{14}$$

$$Q_{ac}^{s}(t)\leq I_{dis}^{s,ac}(t).\sqrt{{S_s}^2-\left(P_{dis}^{s,ac}(t)\right)^2}\forall t \tag{15}$$

$$Q_{ac}^{ev}(t)\leq I_{dis}^{e,ac}(t).\sqrt{{S_e}^2-\left(P_{dis}^{e,ac}(t)\right)^2}\forall t \tag{16}$$

Table IV
NR power flow results comparison between the proposed model and MATLAB/Simulink for grid-connected mode.

	Proposed Model						MATLAB/Simulink					
time	1:00	3:00	5:00	7:00	9:00	11:00	1:00	3:00	5:00	7:00	9:00	11:00
V2	0.999937	0.999724	0.999816	0.999873	0.99954	0.999459	0.999937	0.999723	0.999815	0.999873	0.999539	0.999459
V3	0.999937	0.999724	0.999816	1.001115	1.001798	1.001742	0.999937	0.999723	0.999815	1.001115	1.001797	1.001742
V4	1.000248	1.000458	1.001767	1.00146	0.999851	0.999459	1.000248	1.000458	1.001766	1.001459	0.999850	0.999459
V5	0.999937	1.000741	1.000833	0.999873	0.99954	0.999459	0.999937	1.000740	1.000832	0.999873	0.999539	0.999459
V6	1.001987	0.998186	0.998293	0.998894	0.997705	0.997315	1.001986	0.998185	0.998293	0.998893	0.997704	0.997315
V7	1.000104	0.999314	0.99945	0.999506	0.998301	0.998309	1.000103	0.999313	0.999449	0.999506	0.998300	0.998309
V8	1.000103	0.999317	0.999452	0.99951	0.998377	0.998474	1.000103	0.999316	0.999451	0.999510	0.998376	0.998474
V9	1.000103	0.99891	0.999452	0.999508	0.998104	0.997706	1.000103	0.998910	0.999451	0.999508	0.998104	0.997706
V10	1.001195	0.999317	0.998984	0.999508	0.998308	0.998316	1.001194	0.999316	0.998984	0.999508	0.998307	0.998315
V11	0.999565	0.998991	0.999167	0.999152	0.997718	0.997798	0.999564	0.998991	0.999167	0.999152	0.997718	0.997797
δ2	-0.00315	-0.00928	0.000107	8.99e-5	-0.01475	-0.01598	-0.00314	-0.00927	0.000107	8.98e-05	-0.01474	-0.01598
δ3	-0.00315	-0.00928	0.000107	-9.33e-5	-0.01391	-0.01355	-0.00314	-0.00927	0.000107	-9.3e-05	-0.01390	-0.01354
δ4	-0.00138	-0.00759	0.009761	0.009302	-0.01298	-0.01598	-0.00137	-0.00758	0.009761	0.009302	-0.01297	-0.01598
δ5	-0.00315	-0.00764	0.001748	8.99e-5	-0.01475	-0.01598	-0.00314	-0.00763	0.001748	8.98e-05	-0.01474	-0.01598
δ6	-0.00246	-0.01777	-0.0083	-0.00537	-0.02484	-0.02772	-0.00245	-0.01777	-0.00830	-0.00536	-0.02483	-0.02772
time	14:00	16:00	18:00	20:00	22:00	24:00	14:00	16:00	18:00	20:00	22:00	24:00
V2	0.999973	0.999466	0.999346	0.999519	0.997034	0.997154	0.999973	0.999466	0.999346	0.999519	0.997034	0.997153
V3	1.000573	1.002079	1.001942	1.002774	0.997034	0.997154	1.000573	1.002078	1.001942	1.002773	0.997034	0.997153
V4	0.999973	0.999813	0.999346	0.99983	0.998054	0.998786	0.999973	0.999812	0.999346	0.999830	0.998054	0.998786
V5	0.999973	0.999466	0.999346	1.001627	0.998054	0.995545	0.999973	0.999466	0.999346	1.001626	0.998054	0.995544
V6	1.00248	0.997274	0.99716	0.997406	0.994882	0.994963	1.002479	0.997273	0.997160	0.997405	0.994881	0.994963
V7	1.00035	0.997864	0.997646	0.996798	0.996428	0.997615	1.000350	0.997863	0.997645	0.996798	0.996427	0.997614
V8	1.000546	0.998035	0.997743	0.996815	0.996442	0.997625	1.000546	0.998034	0.997742	0.996815	0.996442	0.997624
V9	1.001526	0.997403	0.997352	0.997095	0.996239	0.998234	1.001525	0.997402	0.997352	0.997095	0.996238	0.998234
V10	1.000349	0.997872	0.997655	0.996811	0.997034	0.996836	1.000348	0.997872	0.997655	0.996811	0.997033	0.996836
V11	0.999759	0.997252	0.996985	0.995876	0.995436	0.996934	0.999759	0.997252	0.996984	0.995876	0.995435	0.996933
δ2	-0.0001	-0.01541	-0.01938	-0.00793	-0.0208	-0.02527	-0.00010	-0.01540	-0.01937	-0.00793	-0.02080	-0.02526
δ3	0.003323	-0.01296	-0.01827	-0.00844	-0.0208	-0.02527	0.003322	-0.01295	-0.01827	-0.00843	-0.02080	-0.02526
δ4	-0.0001	-0.01365	-0.01938	-0.00616	-0.01915	-0.02007	-0.00010	-0.01364	-0.01937	-0.00616	-0.01915	-0.02007
δ5	-0.0001	-0.01541	-0.01938	0.004423	-0.01915	-0.03417	-0.00010	-0.01540	-0.01937	0.004423	-0.01915	-0.03416
δ6	0.002161	-0.02741	-0.03134	-0.01951	-0.03262	-0.03728	0.002160	-0.02740	-0.03134	-0.01951	-0.03261	-0.03728

Table V
NR power flow results comparison between the proposed model and MATLAB/Simulink for islanded mode.

	Proposed Model						MATLAB/Simulink					
time	1:00	3:00	5:00	700	9:00	11:00	1:00	3:00	5:00	7:00	9:00	11:00
V2	0.999893	0.999939	1	0.999928	0.999893	0.999745	0.999893	0.999939	1	0.999928	0.999893	0.999745
V3	0.999896	0.999941	1	1.000172	1.000087	1.00103	0.999896	0.999941	1	1.000172	1.000087	1.00103
V4	1.001018	1.000422	1	1.000211	0.999055	0.999754	1.001018	1.000422	1	1.000211	0.999055	0.999754
V5	0.998887	1.001719	1	0.999931	0.999896	0.999754	0.998887	1.001719	1	0.999931	0.999896	0.999754
V6	1.000306	0.997979	1	0.999757	1.001069	0.999716	1.000306	0.997979	1	0.999757	1.001069	0.999716
V7	0.999975	1.000275	0.999991	1.000014	0.999862	0.999989	0.999975	1.000275	0.999991	1.000014	0.999862	0.999989
V8	0.999975	1.000274	0.999991	1.000016	0.999932	1.000148	0.999975	1.000274	0.999991	1.000016	0.999932	1.000148
V9	1.000788	1.000274	0.999788	1.000014	1.000599	0.999989	1.000788	1.000274	0.999788	1.000014	1.000599	0.999989
V10	0.999396	0.999228	1.000297	1.000014	0.999863	0.999989	0.999396	0.999228	1.000297	1.000014	0.999863	0.999989
V11	0.999867	0.999949	0.999934	0.999943	0.999745	0.999885	0.999867	0.999949	0.999934	0.999943	0.999745	0.999885
$\delta 2$	-0.0002	-0.00011	2.83e-15	-0.00013	-0.0002	-0.00047	-0.0002	-0.00011	2.83e-15	-0.00013	-0.0002	-0.00047
$\delta 3$	-0.0002	-0.00011	2.84e-15	-0.00014	0.001004	0.002125	-0.0002	-0.00011	2.84e-15	-0.00014	0.001004	0.002125
$\delta 4$	0.006873	0.001616	2.84e-15	0.001636	-0.0055	-0.00047	0.006873	0.001616	2.84e-15	0.001636	-0.0055	-0.00047
$\delta 5$	-0.00656	0.011095	2.84e-15	-0.00013	-0.0002	-0.00047	-0.00656	0.011095	2.84e-15	-0.00013	-0.0002	-0.00047
$\delta 6$	8.65e-05	-0.01249	2.84e-15	-0.00123	0.004895	-0.00071	8.65e-05	-0.01249	2.84e-15	-0.00123	0.004895	-0.00071
time	14:00	16:00	18:00	20:00	22:00	24:00	14:00	16:00	18:00	20:00	22:00	24:00
V2	0.999866	1	0.999982	0.999893	1	1	0.999866	1	0.999982	0.999893	1	1
V3	1.000415	1.000449	1.000283	0.999908	1	1	1.000415	1.000449	1.000283	0.999908	1	1
V4	0.999481	1.000723	0.999982	1.000177	1	1	0.999481	1.000723	0.999982	1.000177	1	1
V5	0.999871	1	0.999982	0.999382	1	1	0.999871	1	0.999982	0.999382	1	1
V6	1.000367	0.998829	0.99977	1.000641	1	1	1.000367	0.998829	0.99977	1.000641	1	1
V7	0.999943	1.00015	1.000009	0.993783	0.999968	0.999978	0.999943	1.00015	1.000009	0.993783	0.999968	0.999978
V8	1.000141	1.000312	1.000097	0.993787	0.999968	0.999978	1.000141	1.000312	1.000097	0.993787	0.999968	0.999978
V9	1.000147	0.999361	1.000009	0.993578	1.00033	0.999775	1.000147	0.999361	1.000009	0.993578	1.00033	0.999775
V10	0.999944	1.00015	1.000009	0.99461	0.999968	1.00043	0.999944	1.00015	1.000009	0.99461	0.999968	1.00043
V11	0.999826	1.000026	0.999875	0.993594	0.999767	0.99984	0.999826	1.000026	0.999875	0.993594	0.999767	0.99984
$\delta 2$	-0.00025	2.84e-15	-3.3e-05	-0.0002	2.83e-15	2.83e-15	-0.00025	2.84e-15	-3.39e-5	-0.0002	2.83e-15	2.83e-15
$\delta 3$	0.003183	0.002828	0.001475	-0.00013	2.84e-15	2.84e-15	0.003183	0.002828	0.001475	-0.00013	2.84e-15	2.84e-15
$\delta 4$	-0.00271	0.004556	-3.3e-05	0.00157	2.84e-15	2.84e-15	-0.00271	0.004556	-3.37e-5	0.00157	2.84e-15	2.84e-15
$\delta 5$	-0.00025	2.85e-15	-3.3e-05	-0.00344	2.84e-15	2.84e-15	-0.00025	2.85e-15	-3.37e-5	-0.00344	2.84e-15	2.84e-15
$\delta 6$	2.08e-05	-0.00738	-0.00137	0.002196	2.84e-15	2.84e-15	2.08e-05	-0.00738	-0.00137	0.002196	2.84e-15	2.84e-15

$$Q_{ic}(t) \leq \left(1 - I_{ic}(t)\right).\sqrt{S_{ic}{}^2 - (P_{ic}(t))^2}\forall t \tag{17}$$

Inequality constraints (10)-(12) restrict active power for the main grid, PV system, and IC to their capacities. Eqs. (13)-(17) are reactive power constraints for the utility, PV system, battery-based sources, and IC that explain injected reactive power by converters can follow their reference values as long as they do not exceed corresponding capacity [1,10,11]. Note here, for BESS and EV parking lot, reactive power could be injected to the microgrid only if it is in the discharging mode; and for IC, only if power is transmitted from DC to AC subgrid. Since this paper projects to solve a linear optimization problem, Eqs. (14)-(17) need to be removed from the optimization process. To handle this problem, MATLAB and GAMS applications are linked so that data are transported from the former to the latter. Then GAMS is run, and optimal results are sent back to MATLAB to check converters reactive power constraint for the converters. There, if reactive power value exceeds its limit, converter switches to PQ mode and keep its reactive power upper limit as a new reference. At the end of this section, the interlinking process between

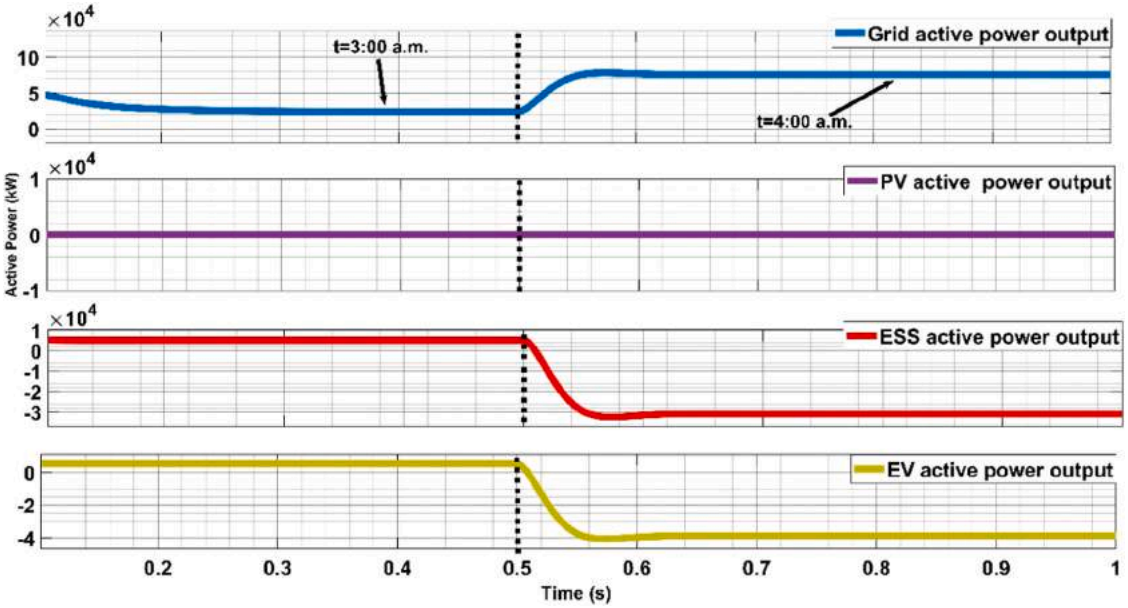

Fig. 15. Active power flow in the AC subgrid.

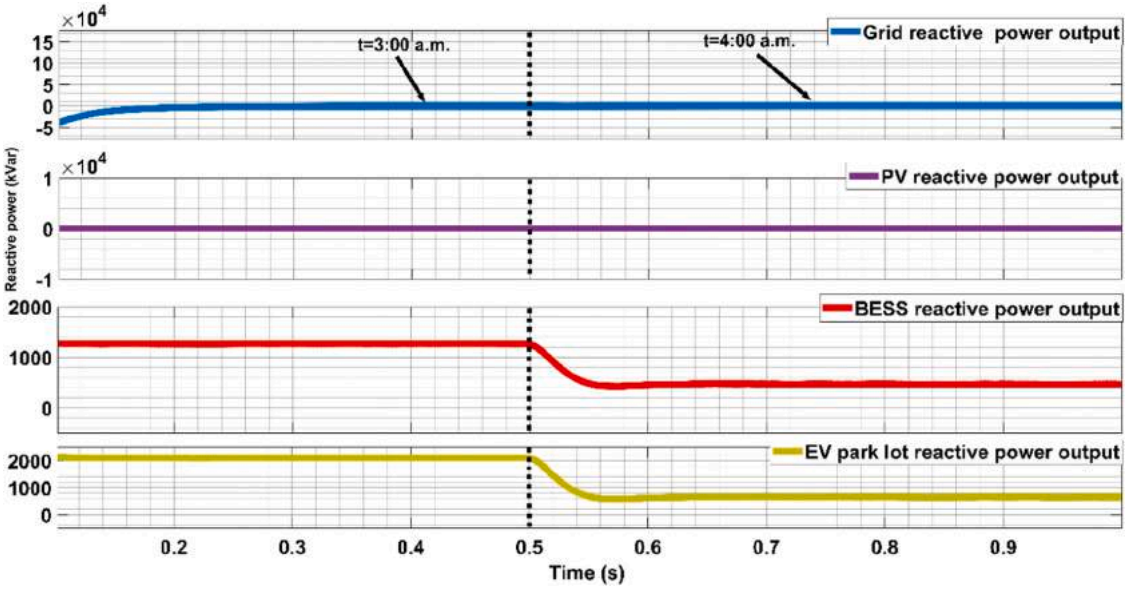

Fig. 16. Reactive power flow in the AC subgrid.

MATLAB and GAMS is outlined. The same optimization algorithm constraints are already used in our last works for self-healing analysis and planning program in AC/DC hybrid microgrids [32] and [33].

Following equations characterize constraints for batteries in BESS and EV station. Inequalities (18)-(25) imply charging/discharging power for the batteries of BESS and EV station in both AC and DC subgrids could not be exceed the corresponding upper and lower limits. Subsequently, (26)-(29) represent that charging and discharging of these batteries might not be done simultaneously through integer variables. Energy available of these sources at each hour are calculated and restricted by (30)-(35). It is vital to consider EVs' batteries are not able to charge or discharge as long as they are out of the lot which are represented in (36) and (37). Finally, constraint (38) makes the optimization program to keep a threshold energy at EVs' batteries at the time they leave the lot.

$$I_{dis}^{s,ac}(t).P_{dis}^{s,\min} \le P_{dis}^{s,ac}(t) \le I_{dis}^{s,ac}(t).P_{dis}^{s,\max}\forall t \tag{18}$$

$$I_{ch}^{s,ac}(t).P_{ch}^{s,\min} \le P_{ch}^{s,ac}(t) \le I_{ch}^{s,ac}(t).P_{ch}^{s,\max}\forall t \tag{19}$$

$$I_{dis}^{s,dc}(t).P_{dis}^{s,\min} \le P_{dis}^{s,dc}(t) \le I_{dis}^{s,dc}(t).P_{dis}^{s,\max}\forall t \tag{20}$$

$$I_{ch}^{s,dc}(t).P_{ch}^{s,\min} \le P_{ch}^{s,dc}(t) \le I_{ch}^{s,dc}(t).P_{ch}^{s,\max}\forall t \tag{21}$$

$$I_{dis}^{e,ac}(t).P_{dis}^{e,\min} \le P_{dis}^{e,ac}(t) \le I_{dis}^{e,ac}(t).P_{dis}^{e,\max}\forall t \tag{22}$$

$$I_{ch}^{e,ac}(t).P_{ch}^{e,\min} \le P_{ch}^{e,ac}(t) \le I_{ch}^{e,ac}(t).P_{ch}^{e,\max}\forall t \tag{23}$$

$$I_{dis}^{e,dc}(t).P_{dis}^{e,\min} \le P_{dis}^{e,dc}(t) \le I_{dis}^{e,dc}(t).P_{dis}^{e,\max}\forall t \tag{24}$$

$$I_{ch}^{e,dc}(t).P_{ch}^{e,\min} \le P_{ch}^{e,dc}(t) \le I_{ch}^{e,dc}(t).P_{ch}^{e,\max}\forall t \tag{25}$$

$$I_{dis}^{s,ac}(t) + I_{ch}^{s,ac}(t) \le 1\forall t \tag{26}$$

$$I_{dis}^{s,dc}(t) + I_{ch}^{s,dc}(t) \le 1\forall t \tag{27}$$

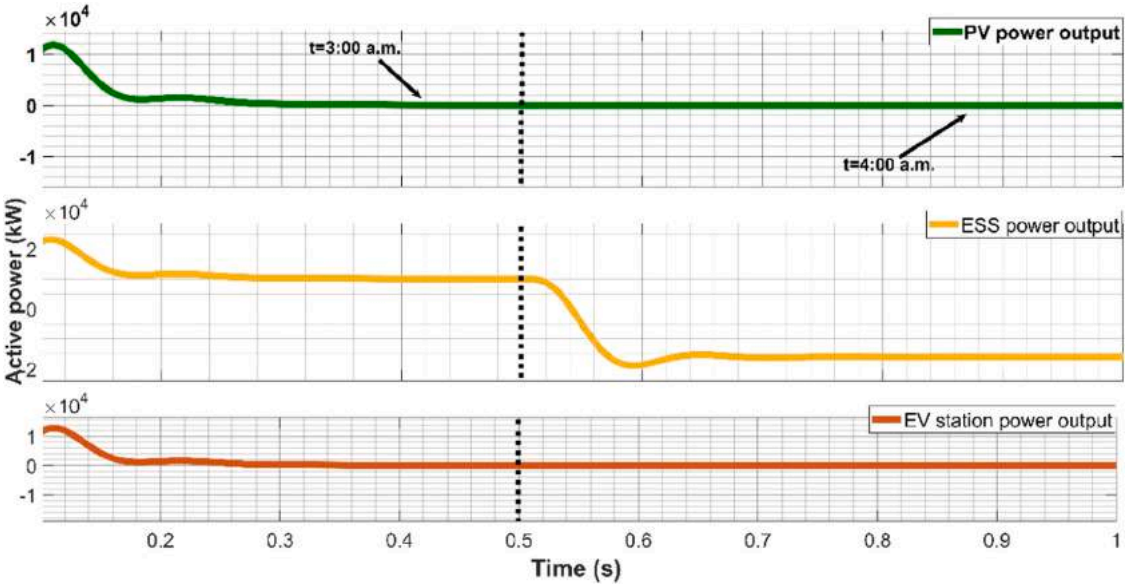

Fig. 17. Active power flow in the DC subgrid.

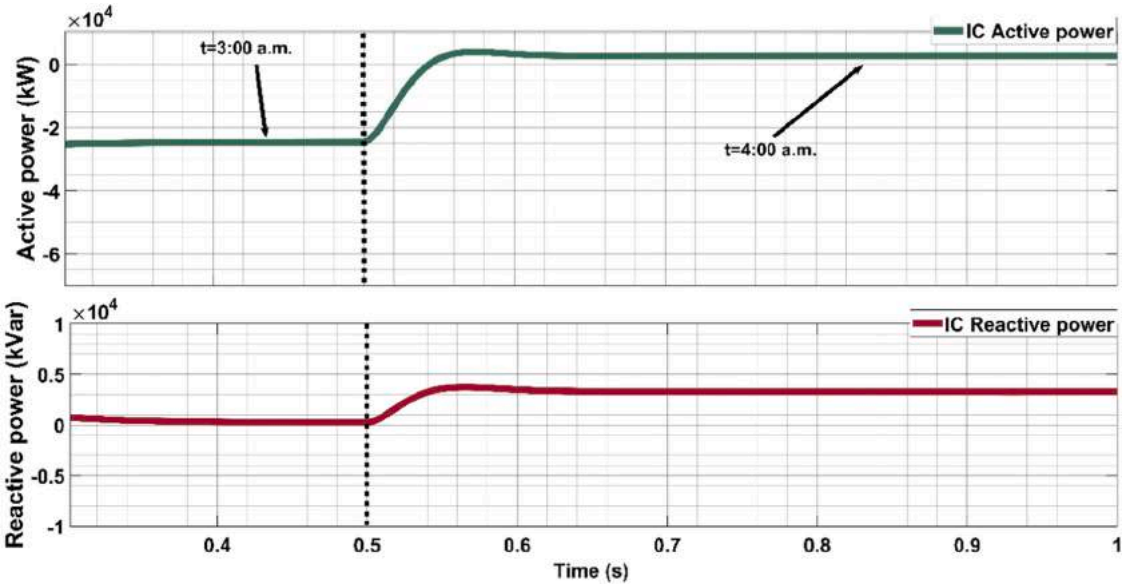

Fig. 18. Active and reactive power flow in the IC.

$$I_{dis}^{e,ac}(t) + I_{ch}^{e,ac}(t) \leq 1 \forall t \quad (28)$$

$$I_{dis}^{e,dc}(t) + I_{ch}^{e,dc}(t) \leq 1 \forall t \quad (29)$$

$$E_{ac/dc}^{s}(t) = E_{ac/dc}^{s}\left(t-1\right) + Q.P_{ch}^{s,ac/dc}(t) - P_{dis}^{s,ac/dc}(t)\Big/Q \quad \forall t > 1 \quad (30)$$

$$E_{ac/dc}^{s}(t) = U_{ac/dc}^{s}(0) + Q.P_{ch}^{s,ac/dc}(t) - P_{dis}^{s,ac/dc}(t)\Big/Q \quad \forall t < 2 \quad (31)$$

$$E_{s}^{\min} \leq E_{ac/dc}^{s}(t) \leq E_{s}^{\max} \forall t \quad (32)$$

$$E_{ac/dc}^{e}(t) = E_{ac/dc}^{e}\left(t-1\right) + Q.P_{ch}^{e,ac/dc}(t) - P_{dis}^{e,ac/dc}(t)\Big/Q \quad \forall t > 1 \quad (33)$$

$$E_{ac/dc}^{e}(t) = U_{ac/dc}^{e}(0) + Q.P_{ch}^{e,ac/dc}(t) - P_{dis}^{e,ac/dc}(t)\Big/Q \quad \forall t < 2 \quad (34)$$

$$E_{e}^{\min} \leq E_{ac/dc}^{e}(t) \leq E_{e}^{\max} \forall t \quad (35)$$

$$P_{dis}^{e,ac/dc}(t) = 0 \forall t \in T_{out} \quad (36)$$

$$P_{ch}^{e,ac/dc}(t) = 0 \forall t \in T_{out} \quad (37)$$

$$E_{ac/dc}^{e}(t_l) \geq N.\lambda.D \quad (38)$$

4.2. Islanded mode

Microgrids could be disconnected from the main grid at PCC, in this case, hybrid microgrid needs to operate autonomously. Assuming there might not be sufficient available energy from generators to supply all loads at specific hours, operators must conduct a proper load shedding to implement a stable and reliable operation. Therefore, in islanded mode, the objective function of the tertiary level controller is minimizing total load shedding rates as:

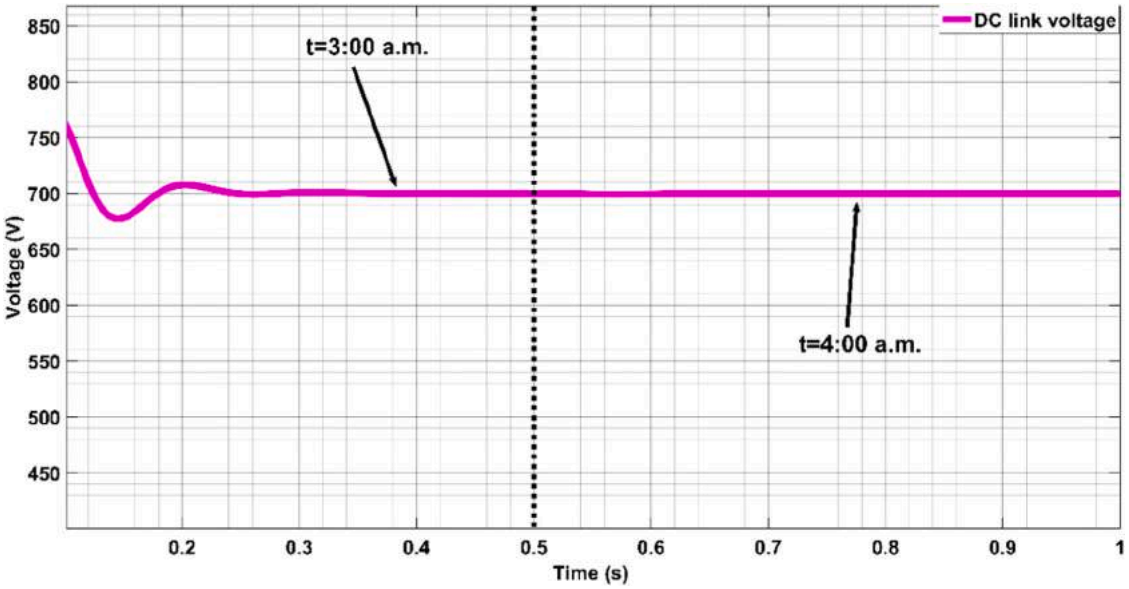

Fig. 19. DC link voltage connected to IC.

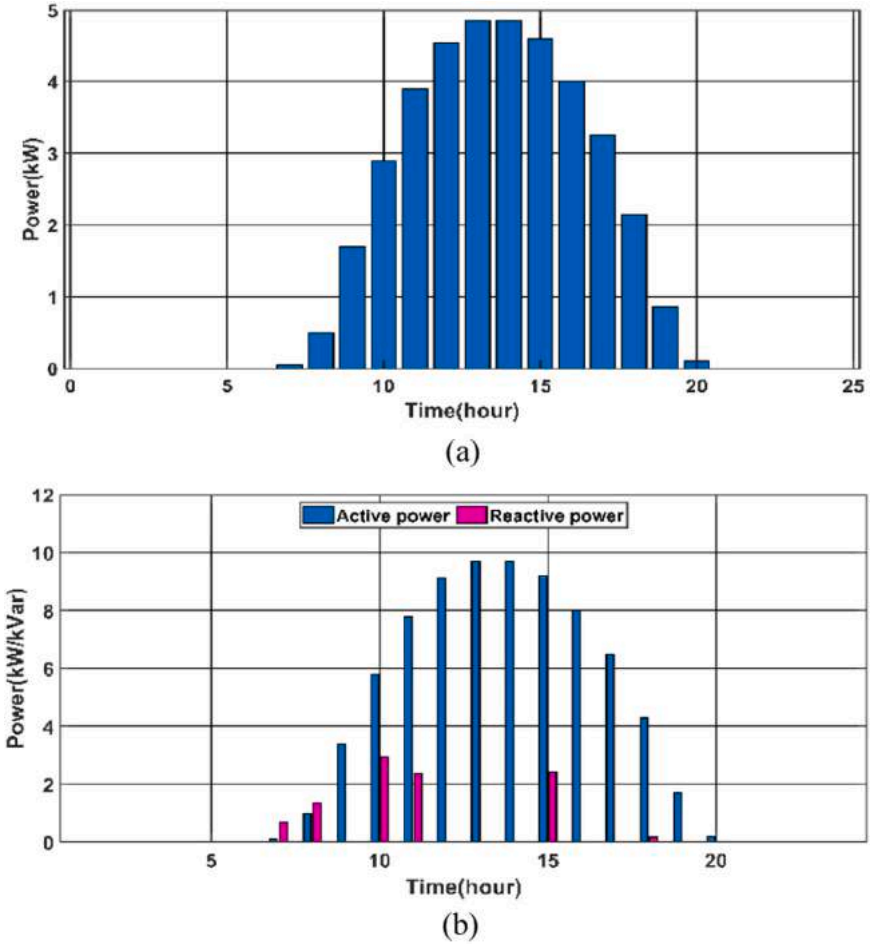

Fig. 20. Hourly power generated by PV system: (a) DC grid, (b) AC grid.

$$L_T^{sh} = \sum_{t=1}^{24} \gamma^{ac}(t).\left(P_l^{ac}(t) + Q_l^{ac}(t)\right) + \gamma^{dc}(t).P_l^{dc}(t)\forall t \tag{39}$$

Constraints in this scenario are like those for grid-connected mode but there is no more power from the main grid. In addition, to minimize the load shedding rates, converters connected to PV systems operate in MPPT control mode. Load demand in power balance set equations is modified as follows:

$$\begin{cases} P_{l,i}^{ac}(t) = \left(1 - \gamma^{ac}(t)\right).P_l^{ac}(t) \\ Q_{l,i}^{ac}(t) = \left(1 - \gamma^{ac}(t)\right).Q_l^{ac}(t)\,\forall t \\ P_{l,i}^{dc}(t) = \left(1 - \gamma^{dc}(t)\right).P_l^{dc}(t) \end{cases} \tag{40}$$

4.3. NR power flow problem

To model NR power flow analysis in AC grids, buses need to be defined as one of the three types of buses including slack bus with voltage magnitude and phase angle are 1 and 0 respectively, which here it is the bus connected to the main grid in grid connected mode, *PV* buses with fixed active power generation and voltage magnitude, and the last type is *PQ* or load buses with scheduled active and reactive power. In this paper, all converter buses are referred as load ones where schedule powers come from the tertiary level, and PCC bus and DC link are load buses connecting to AC and DC loads, and corresponding AC system frequency and voltage are regulated by the main grid. For a bus in AC subsystem, the injected active and reactive power are calculated as follows:

$$\begin{aligned} P_n^{ac} =& |V_n|^2 G\left(n,n\right) + \sum_{\substack{j\in\Omega_{ac} \\ j\neq n}} |V_n||V_m|G(n,m)\cos(\delta_n - \delta_m) \\ &+ |V_n||V_m|B(n,m)\sin(\delta_n - \delta_m)\forall t \end{aligned} \tag{41}$$

$$\begin{aligned} Q_n^{ac} =& -|V_n|^2 B\left(n,n\right) + \sum_{\substack{j\in\Omega_{ac} \\ j\neq n}} |V_n||V_m|G(n,m)\sin(\delta_n - \delta_m) \\ &- |V_n||V_m|B(n,m)\cos(\delta_n - \delta_m)\forall t \end{aligned} \tag{42}$$

where *n* and *m* represent the different buses of the AC system, and *G and B* are respectively conductance and susceptance of the admittance matrix. In DC subgrid, however, there are only two categories for buses: P/load bus or V bus with fixed voltage magnitude. Due to the lack of frequency in DC grid, formulation for calculated active power is the following equation where admittance matrix has only conductance part *g*.

$$P_n^{dc} = |V_n|^2 g\left(n,n\right) + \sum_{\substack{j\in\Omega_{dc} \\ j\neq n}} |V_n||V_m|g(n,m)\forall t \tag{43}$$

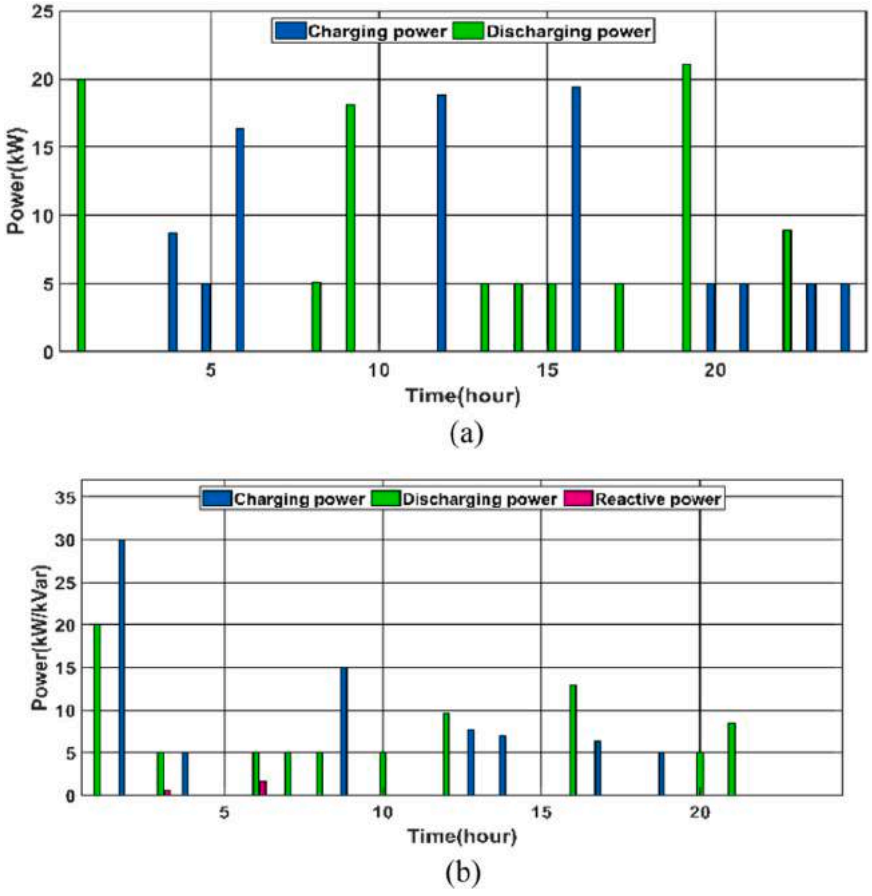

Fig. 21. Hourly power generated by BESS system: (a) DC grid, (b) AC grid.

Expanding (41)-(43) in Taylor's series about the initial estimate and neglecting all higher order terms, a set of linear equations as follows is extracted to calculate the difference between calculated and scheduled power and solved iteratively.

$$\begin{bmatrix} \Delta P^{ac} \\ \Delta Q^{ac} \\ \Delta P^{dc} \end{bmatrix} = \begin{bmatrix} \frac{\partial P^{ac}}{\partial \delta} & \frac{\partial P^{ac}}{\partial |V_{ac}|} & \frac{\partial P^{ac}}{\partial V_{dc}} \\ \frac{\partial Q^{ac}}{\partial \delta} & \frac{\partial Q^{ac}}{\partial |V_{ac}|} & \frac{\partial Q^{ac}}{\partial V_{dc}} \\ \frac{\partial P^{dc}}{\partial \delta} & \frac{\partial P^{dc}}{\partial |V_{ac}|} & \frac{\partial P^{dc}}{\partial V_{dc}} \end{bmatrix} \begin{bmatrix} \Delta \delta \\ \Delta |V_{ac}| \\ \Delta V_{dc} \end{bmatrix} \tag{44}$$

Note that for the AC bus connected to IC, scheduled active power is calculated by Eq. (3), which is the same for DC bus connected to IC with opposite sign since power losses in IC is neglected. For the case that active power is injected to DC grid, this calculated active power is considered as a generation power for DC link, and, inversely, it adds to the DC load when power is transferred from DC to AC grid. Reactive power for the AC bus connected to IC, however, comes from the optimization program. The interlinking process between MATLAB and GAMS is illustrated in Fig. 7. Initially, data is loaded into MATLAB, followed by its transfer to GAMS. The tertiary level is addressed using Mixed Integer Linear Programming (MILP) via GAMS Cplex solver, then the optimal load sharing results, including scheduled active and reactive powers for all resources, are sent back from GAMS to MATLAB, where power flow problem is solved. Before solving PF, MATLAB checks the non-linear constraints (14)-(17) in each power flow iteration. By doing this, there is no need to run a non-linear optimization in GAMS, as PF is inherently a non-linear problem. If the reactive power value exceeds its limit, converter switches to PQ mode and keep its reactive power upper limit as a new reference. Then, new data is sent again to GAMS to solve a new optimization problem.

5. Case study analysis

Fig. 8 shows an 11-bus AC/DC hybrid microgrid that is going to be installed for Italian pilot as a part of a project named HYPERRIDE. This microgrid is a part of Italian distribution system where is connected to the distribution station ASM at PCC (bus #2) through line 1 at 400 V, while ± 700 V DC lines are constructed in DC subgrid. In both AC and DC sides, there are PV systems as RESs, and the base apparent power is 100 kVA. In addition, flexible resources such as BESSs and EV stations are available in both subgrids. AC/DC converters are connected to the PCC bus through LCL filter, meanwhile DC ones are connected to the DC link (bus #7) via dc resistances [34]. IC couples both subgrids to share powers between them and help DC link voltage regulation in both operation modes. In islanded operating mode, the IC is also projected to transfer power between both AC and DC subgrids to guarantee power balance, where AC voltage and frequency restoration is reached.

Since this microgrid has not been operated yet, hourly load data, irradiance to calculate PV output power, and EVs data are not available; therefore, corresponding data for another part of Italian distribution systems are used referring to the database from ARERA, the Italian Regulatory Authority for Energy, Networks and the Environment providing the most recent technical reports on the energy transition in Europe and Italy [35–39]. This problem does not reduce the effectiveness and application of this work because a general and robust model has been proposed that may be conducted to any hybrid systems. The pattern for load consumption, and maximum generation of PV systems in a 24-hours day in April for the proposed case study are illustrated in Fig. 9, where these values are in per unit (p.u.) system. However, the capacity of converters connected to PV, BESS, and EV station systems,

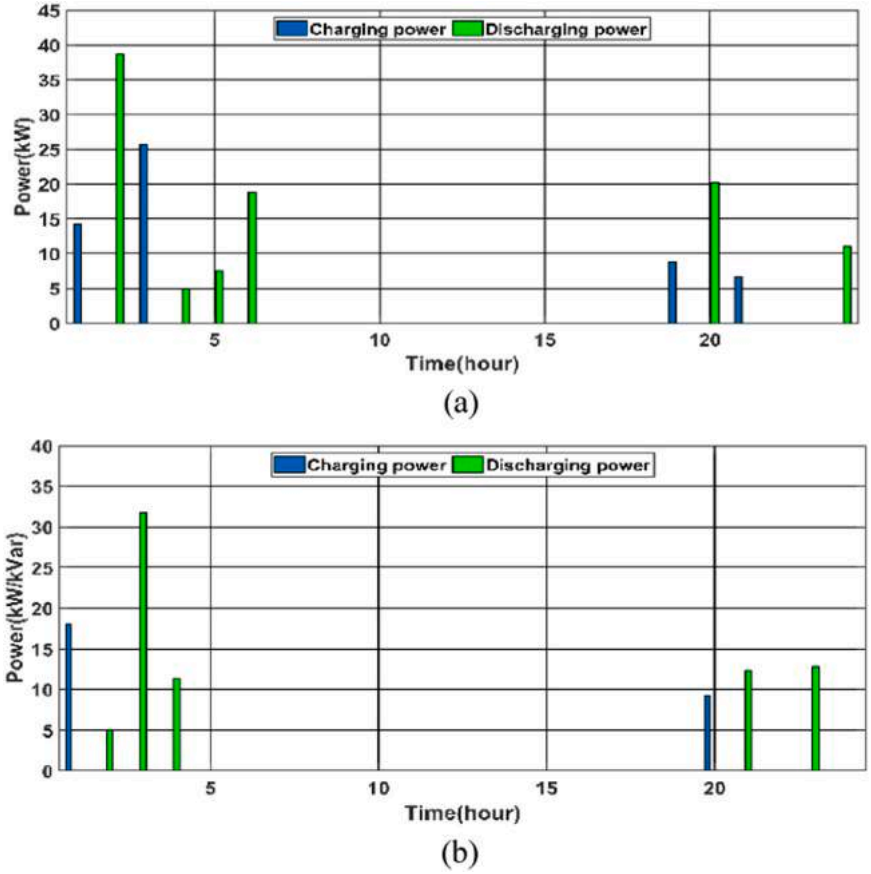

Fig. 22. Hourly power generated by EV parking lot: (a) DC grid, (b) AC grid.

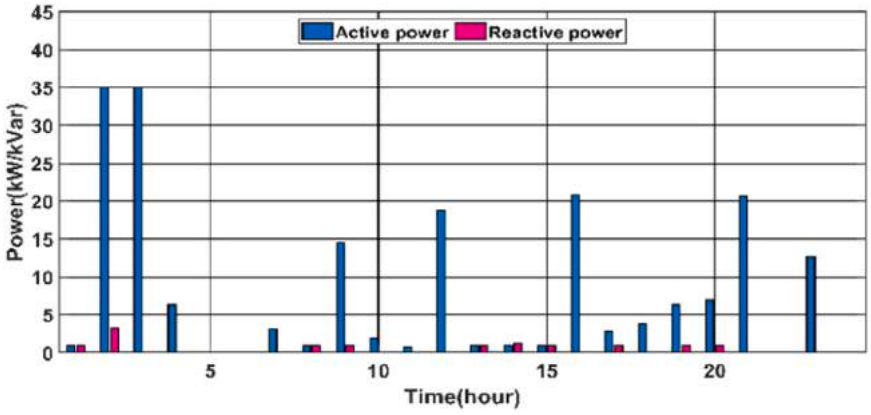

Fig. 23. Hourly power exchange between AC and DC grids through IC.

and peak loads consumption have been designed and reported in [34] and presented at Table II. In AC and DC subgrids, there is a small-scale parking lots for EVs each including five mid-size sedans with 10 kWh battery capacity, means that maximum available energy at each lot is 50 kWh. It is assumed that charging station is a fast charge type so that each EV could be fully recharged by one hour; therefore, maximum charge/discharge power is 50 kW at each time interval. In this paper, the efficiency of converters in BESSs and EV parking lots is 95%.

Energy price is one of the most noticeable parameters that could affect considerably the pattern of charging/discharging of the flexible resources, power purchased from the main grid, and finally power generated by the RESs and power flow calculations. In addition, it is clear that this parameter varies depending on the weekdays and the time a day. Therefore, taking a realistic energy price into account leads to improvement of the analysis. Table III represents the energy price for different days and hours in the Italian market in 2023.

To conduct a more close-to-real model for EVs, many authors have implemented stochastic approaches like Monte Carlo Simulation (MCS) to characterize the pattern of leaving and arriving time at lots, and journey distance each day. These models are practical for the cases with a lot of EVs, while there is only a small fleet with five EVs. On the other hand, since this paper aims to calculate daily power flow and considers the buses connected to EVs stations as load ones, it is required to have an active and a reactive power reference, while stochastic models aim to

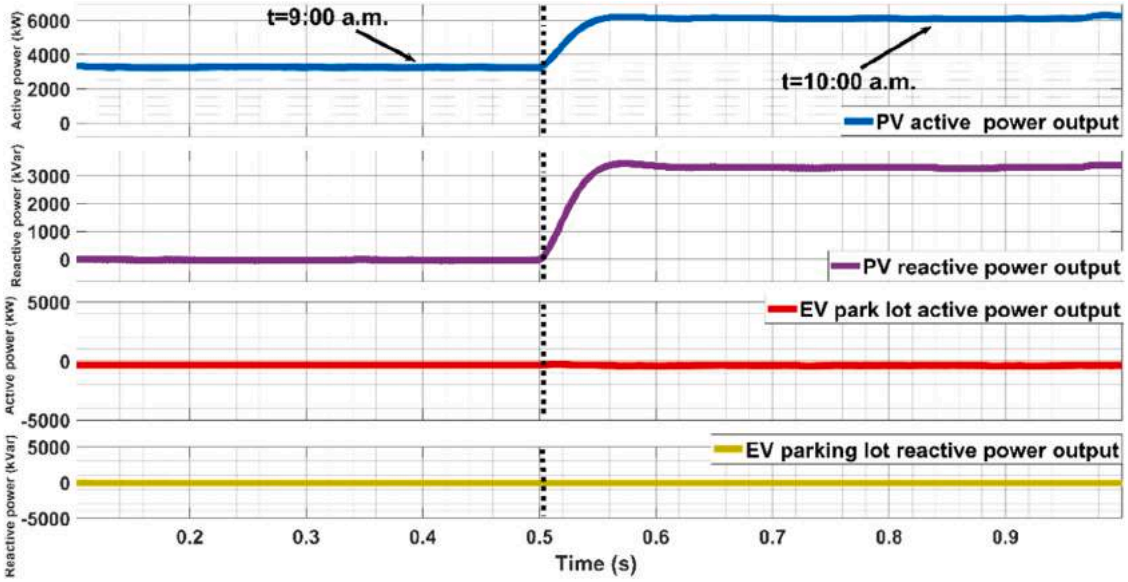

Fig. 24. Active and reactive powers of PV system and parking lot in AC side.

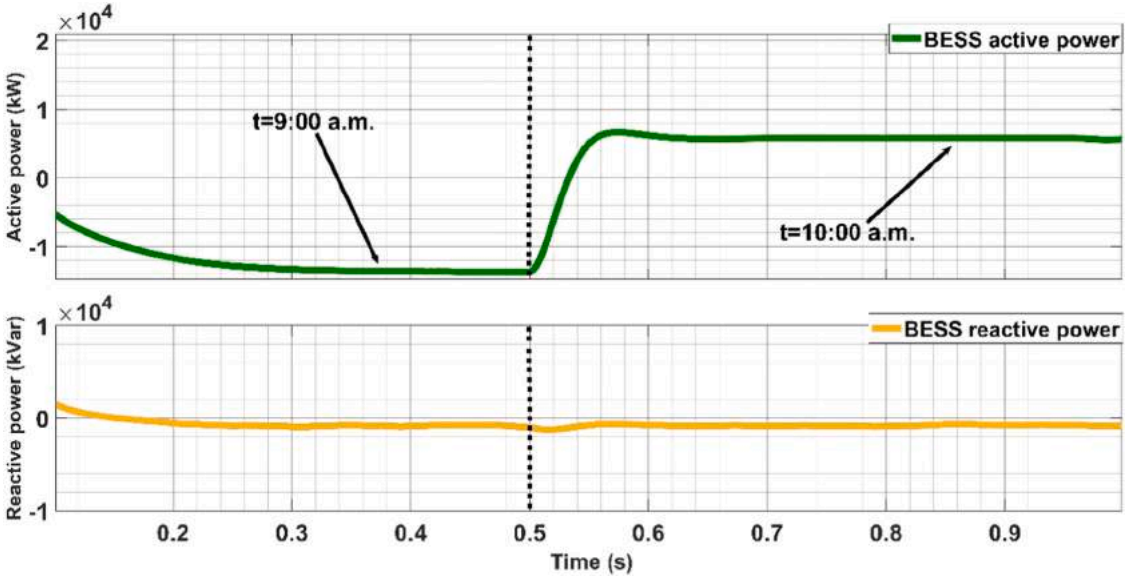

Fig. 25. Active and reactive powers of BESS in AC side.

evaluate the effect of unpredictable specifics of EVs on other parameters. Therefore, deterministic pattern for EVs is proposed in this paper, where it is assumed leaving and arriving time for these vehicles are 7:00 and 19:00, respectively. The average trip distance each day is 10 km and the initial energy available (state of charge) in EVs' batteries and BESS is 60% of the total capacity meaning 5 and 30 kWh each subgrid.

5.1. Power flow analysis in grid-connected mode

In this section, power flow problem is solved for 24 hours a day in grid-connected mode. First, tertiary controller, that is an optimization program, is solved, then active and reactive power generation by photovoltaic systems, and generation/consumption powers by BESS and EVs are called and sent to the operator to calculate power flow, and to the local controllers of the converters to perform primary control. It is worth to mention that local devices measure the frequency at PCC and dc voltage at DC link utilizing Eq. (3) to calculate active power transferred through the interlinking converter. Starting with the tertiary level, Figs. 10–13 illustrate the active and reactive powers generated by different sources for a day.

Fig. 10 shows the active and reactive power purchased from the main grid. Figs. 11–13 depict power generated by PV systems, charging/discharging powers at BESSs units and EV parking lots, respectively, for both DC and AC subsystems. Looking at Fig. 12 and Fig. 13, it is clear that charging and discharging could not be issued simultaneously, and the corresponding converters at the AC grid inject reactive power only in discharging modes (see Fig. 12 (b) and Fig. 13 (b)). In addition, Fig. 14 depicts the hourly active and reactive power exchange between AC and DC subgrids through the interlinking converter, where only at 1:00, 4:00, 6:00, 8:00 and 14:00 DC subgrid injects active and reactive power to the AC one. It is expected because DC grid has higher load demand than AC one (see Table II).

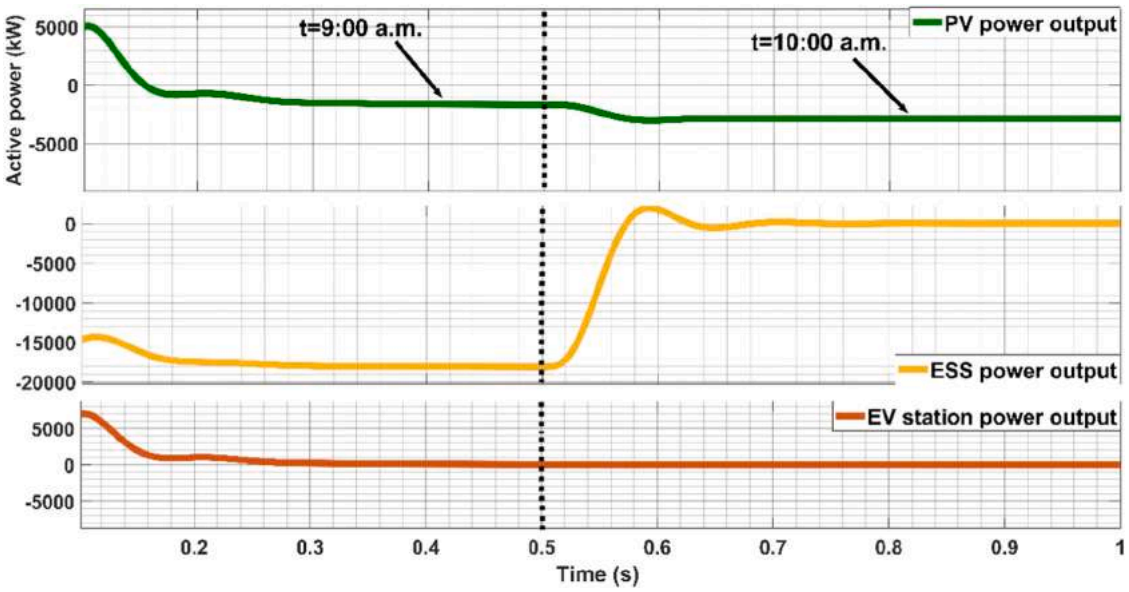

Fig. 26. Active power flow in DC subgrid.

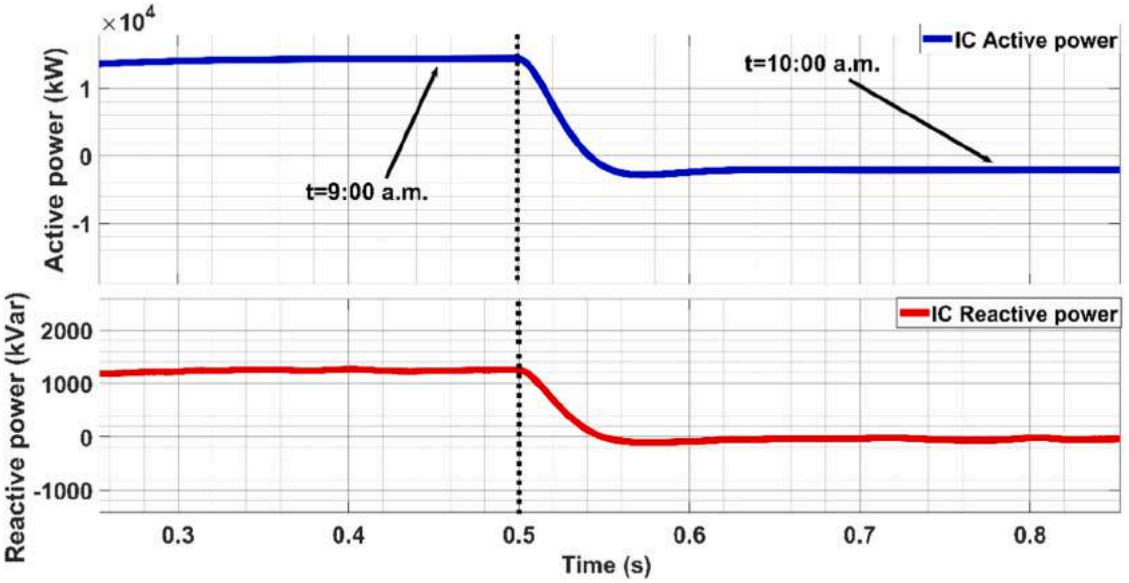

Fig. 27. Active and reactive power flow in the IC.

At each hour, scheduled (reference) active and reactive powers for buses #3–5 in AC grid and active scheduled power for buses #8–10 in DC side come from the tertiary level (Figs. 11–13). Reactive powers in Fig. 14 are utilized as the scheduled values for the bus #6 connected to the AC side of the IC, while the corresponding scheduled active power is calculated via Eq. (3). PCC bus #2, DC link bus #7, and bus #11 are considered as PQ/load buses with fixed hourly demands and negative scheduled active and reactive powers. Bus #1 is a slack connection with voltage magnitude 1 p.u. and phase angle 0. NR power flow model is implemented at each hour a day for the case study. Table IV presents a comparison between power flow results for the proposed model and MATLAB/Simulink (power flow tool) including voltage magnitudes in p. u. and phase angles in radian. First column indicates Vn and δn which are voltage and phase angle of nth bus. The proposed power flow model is run by about 0.0155 second that is sufficiently fast. The simulation is run for 2 seconds, representing almost steady-state since voltage magnitudes and phase angles match those from the proposed model shown at Table IV with an error 4.0051e-11.

In addition, to show how converters' controllers work perfectly in steady-state, for both grid-connected and islanded modes a two-hour time interval is set each. To accomplish this, the microgrid under study, PV-storage systems, and parking lots, along with the corresponding controllers for the converters (Figs. 2–6), are designed and simulated using MATLAB/Simulink for two purposes. First, to demonstrate that the controllers work perfectly by following the references powers coming from the optimization in both grid-connected and islanded modes. It also proves that storage system in AC subgrid perfectly regulates voltage and frequency at PCC in islanded mode. Second, power flow toll in Simulink is used to perform power flow analysis, validating the power flow results from the proposed model (Tables IV and V). In grid-connected operation mode, the simulation results, relating powers transferred through converters and dc link

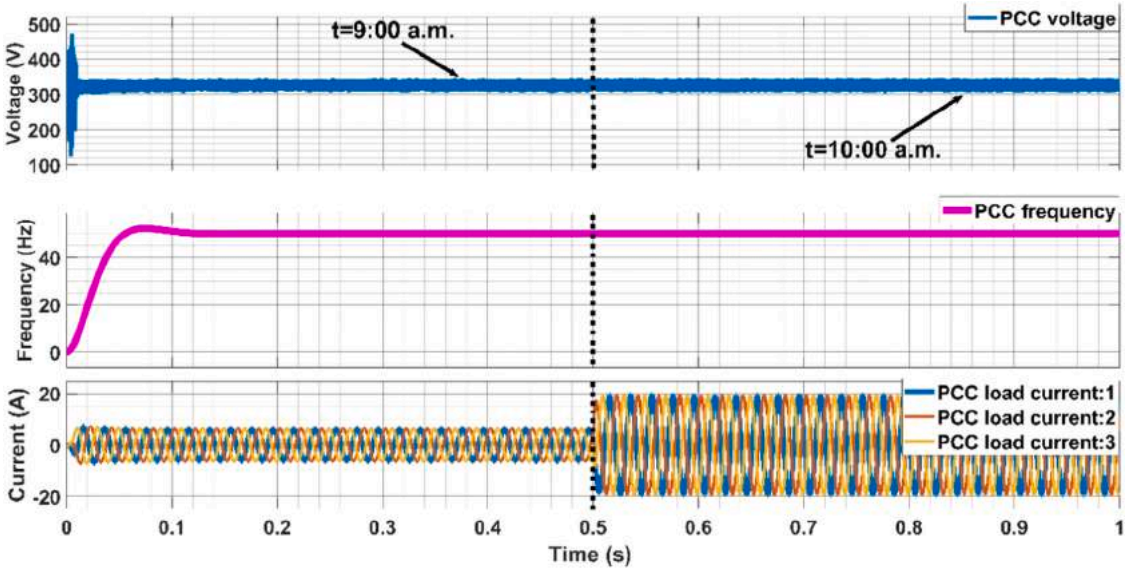

Fig. 28. Voltage, frequency, and load current at PCC.

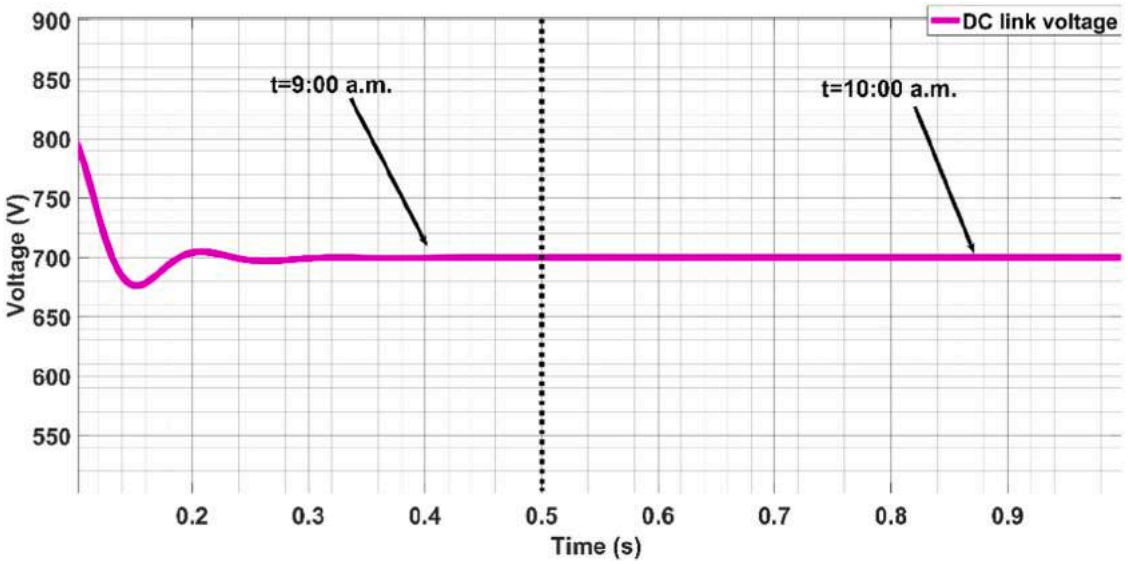

Fig. 29. DC link voltage.

voltage, are exploited for 1 second, where the first half second represents the powers for the first hour, while the second half relates to the second hour of the time interval. Figs. 15- 17 show active and reactive powers imported from the main grid, and those from the PV, BESS and EV lot, respectively, in the AC and DC subgrids at the time interval 3:00–4:00 a.m. Comparing these figures to Figs. 10–13, the powers imported from the main grid, PV generation, charging/discharging powers of the converters in BESS and EV parking lots perfectly match the set points that the tertiary controller sends to the local controllers. Note that PV systems in both AC and DC subsystems cannot generate power from 3:00–4:00 a.m. The storage system and parking lot in the AC subgrid start discharging (positive power) at 3:00, followed by discharging (negative power) at 4:00. In the DC subgrid, only BESS is active. It is first charged (power with a positive sign) and then starts discharging (negative power). Once all DGs follow the reference powers, the main grid injects active and reactive powers based on the values from optimization.

These converters operate in current constant mode so that the corresponding controllers follow the references powers from the tertiary level. Figs. 18 and 19 depict the power exchange between two AC and DC subgrids through IC and dc link voltage respectively. IC follows a constant current mode where the reference active power is calculated by difference between normalized frequency and dc voltage leading to a stable dc voltage. In this case, at 3:00 active power is transferred from the AC side to the DC one (zero reactive power), whereas at 4:00 active and reactive powers are injected to the ac grid from the DC one.

5.2. *Power flow analysis in islanded mode*

Hierarchal power flow analysis is also conducted for the case study in islanded operating mode. To avoid repetitious expressions, only results and analysis related to islanded mode are discussed. In this case, AC/DC hybrid grid is disconnected from the main grid. As it is discussed in the section III, in islanded mode, PV systems and flexible sources may not

supply total AC and DC loads at each hour. So, tertiary level optimizes the rate of load shedding so that the remind load could be powered. In such a case, converters connected to the PV systems, EV parking lots, BESS in DC system, and the IC follow the same corresponding control modes as those in grid-connected mode, but BESS in the AC grid switches to voltage source mode where it tries to follow the reference powers aiming to keep voltage and frequency in the reference values at PCC bus. Starting with the tertiary level, Figs. 20–23 illustrate the active and reactive powers generated by different sources for a day. The note is that, since the hybrid grid is disconnected from the main grid, load consumption in DC grid is lower than AC one as well, IC injects active and reactive power to AC grid more hours than in grid-connected operating mode (see Fig. 23).

Power flow calculations by the proposed model and simulation are reported in Table V. Like in grid-connected mode, power flow results by simulation match those from the model perfectly by an error 2.0007e-13, where the proposed model takes 0.013 second which is meaningfully fast.

To assess the behavior of the primary controller of the converters in islanded mode, the controlled hybrid AC/DC grid is simulated for one second (like that in grid-connected mode) in the period 9:00–10:00 a.m. using MATLAB/Simulink. Corresponding power outputs are illustrated in Figs. 24–27. Comparing these figures to Figs. 20–23, PV generation, charging/discharging powers of the converters in BESS and EV parking lots perfectly match the set points that the tertiary controller sends to the local controllers. Looking at Fig. 25, at 9:00 a.m. BESS is charged at a value lower than the reference point, while at 10:00 it starts discharging where its power output is a little higher than the reference value to keep voltage and frequency at

PCC close to their nominal values. Voltage, frequency, and load current at PCC are depicted in Fig. 28, DC link voltage is shown in Fig. 29 as well. Although the operation mode of BESS, the rate of loads, and injected power direction at IC are changed for two hours, voltage and frequency at PCC and DC link voltage remain stable.

6. Conclusion

This paper proposes a power flow analysis for a two-level controlled AC/DC hybrid microgrid in both grid-connected and islanded operating modes. In grid-connected mode, the tertiary level controller, playing energy management system role, minimizes the daily cost of the energy purchased from the utility, leading to active and reactive power references calculation. These scheduled power set-points are then sent to the converters' controller connected to the RESs and the flexible resources and are used in Newton-Raphson power flow calculations. Local controller adopts current control mode as the primary controller to generate and follow the power references. In islanded mode, however, tertiary level tries to minimize the load shedding to obtain a stable and reliable load supply. To keep a stable voltage and frequency in the AC system, the converter connected to the storage system implements P-ω/Q-V droops to generate voltage and frequency references, meanwhile tries to produce powers close to the corresponding references. Other sources, however, remain in current control mode. In both operation modes, interlinking converter plays the most significant role to transmit power between two grids. The difference between DC link voltage and frequency is used as a droop control to identify the direction of injected power so that voltage of dc link and frequency at PCC (especially in islanded mode) are kept stable. Power flow equations are solved using the unified NR technique sufficiently fast. Results from the optimization program are obtained for the proposed case study and shown at bar charts. In islanded mode, it is noticeable that some loads must be shedded since RESs and storage systems may not power them. Power flow analysis results from simulated hybrid grid by Simulink perfectly match with those from the NR model with a high accuracy. In addition, control schemes are simulated and results at graphs represent controllers precisely follows the set points came from the optimization level, and the converter connected to the AC storage system keep voltage and frequency stability in islanded mode. The point is that the proposed methodology is a general model applicable to real existing grids with diverse configurations comprising various resources and loads. These highlights mentioned above prove the effectiveness, precision model with a sufficient convergence speed. Power flow analysis model proposed in this paper could be implemented for other vital issues in power systems such as fault and cascading failure analysis, stability, among others, where cascading failure analysis is going to be the next authors' research interest.

CRediT authorship contribution statement

Eleonora Riva Sanseverino: Resources, Project administration. **Josep M. Guerrero:** Resources, Project administration, Supervision. **Gaetano Zizzo:** Writing – review & editing, Supervision, Investigation. **Juan C. Vasquez:** Supervision, Resources, Methodology, Investigation. **Gibran David Agundis Tinajero:** Writing – review & editing, Software, Methodology. **Salar Moradi:** Writing – original draft, Visualization, Software, Methodology, Data curation, Conceptualization.

Declaration of Competing Interest

The authors declare that they have no known competing financial interests or personal relationships that could have appeared to influence the work reported in this paper.

Data availability

Data will be made available on request.

Acknowledgements

We would like to thank Center for Research on Microgrids (CROM) in energy department at University of Aalborg (AAU) where this article was projected at, as well as staff at AAU for administrative support. Professors Tinajero and Vasquez are gratefully thanked for supervising this work, and Prof. Guerero is gratefully acknowledged for leadership. We also appreciate university of Palermo, especially Prof. Eleonora Riva Sanseverino (coordinator of energy department), for providing us this opportunity to have a collaboration with CROM.

References

[1] H.M.A. Ahmed, A.B. Eltantawy, M.M.A. Salama, A planning approach for the network configuration of AC-DC hybrid distribution systems, IEEE Trans. Smart Grid vol. 9 (3) (May. 2018) 2203–2213.
[2] J. Guerrero, J. Vasquez, J. Matas, L. De Vicuña, M. Castilla, Hierarchical control of droop-controlled AC and DC microgrids-wa general approach toward standardization, IEEE Trans. Ind. Electron. vol. 58 (1) (Jan. 2011) 158–172.
[3] P.C. Loh, D. Li, Y.K. Chai, F. Blaabjerg, Autonomous control of interlinking converter with energy storage in hybrid AC–DC microgrid, IEEE Trans. Ind. Appl. vol. 49 (3) (May/Jun. 2013) 1374–1382.
[4] L. Che, M. Shahidehpour, A. Alabdulwahab, Y. Al-Turki, Hierarchical coordination of a community microgrid with AC and DC microgrids, IEEE Trans. Smart Grid vol. 6 (6) (Nov. 2015) 3042–3051.
[5] M. Abdelaziz, H. Farag, E. El-Saadany, Y.-R. Mohamed, A novel and generalized three-phase power flow algorithm for islanded microgrids using a newton trust region method, IEEE Trans. Power Syst. vol. 28 (1) (Feb. 2013) 190–201.
[6] S. Chopra, G.M. Vanaprasad, G.D.A. Tinajero, N. Bazmohammadi, 1214 J. C. Vasquez, J.M. Guerrero, Power-flow-based energy man- 1215 agement of hierarchically controlled islanded AC microgrids, Int. J. 1216 Electr. Power Energy Syst. vol. 141 (Oct. 2022) 108140 (Art. no).
[7] M.H. Moradi, V.B. Foroutan, M. Abedini, Power flow analysis in islanded microgrids via modeling different operational modes of DGs: A review and a new approach, Renew. Sustain. Energy Rev. vol. 69 (Mar. 2017) 248–262.
[8] G. David, A. Tinajero, M. Nasir, J.C. Vasquez, J.M. Guerrero, Comprehensive power flow modelling of hierarchically controlled AC/DC hybrid islanded microgrids", Int. J. Electr. Power Energy Syst. vol. 127 (May 2021).
[9] H.M.A. Ahmed, A.B. Eltantawy, M.M.A. Salama, A generalized approach to the load flow analysis of AC–DC hybrid distribution systems, IEEE Trans. Power Syst. vol. 33 (2) (Mar. 2018) 2117–2127.

[10] E. Aprilia, K. Meng, M. Al-Hosani, H.H. Zeineldin, Z.Y. Dong, Unified Power Flow Algorithm for Standalone AC/DC Hybrid Microgrids, IEEE Trans. Smart Grid vol. 10 (1) (Jan. 2019) 639–649.
[11] A.A. Hamad, M.A. Azzouz, E.F. El Saadany, A Sequential Power Flow Algorithm for Islanded Hybrid AC/DC Microgrids, IEEE Trans. Power Syst. vol. 31 (5) (Sept. 2016) 3961–3970.
[12] F. Mumtaz, M.H. Syed, M.A. Hosani, H.H. Zeineldin, A novel approach to solve power flow for islanded microgrids using modified Newton Raphson with droop control of DG, IEEE Trans. Sustain. Energy vol. 7 (2) (Apr. 2016) 493–503.
[13] M.E. Nassar, A.A. Hamad, M.M.A. Salama, E.F. El-Saadany, A Novel Load Flow Algorithm for Islanded AC/DC Hybrid Microgrids, IEEE Trans. Smart Grid vol. 10 (2) (Mar. 2019) 1553–1566.
[14] A.A. Eajal, M.A. Abdelwahed, E.F. El-Saadany, K.A. Ponnambalam, Unified Approach to the Power Flow Analysis of AC/DC Hybrid Microgrids, IEEE Trans. Sustain. Energy vol 7 (3) (July 2016) 1145–1158.
[15] G. Agundis-Tinajero, et al., Extended-optimal-power-flow-based hierarchical control for islanded AC microgrids, IEEE Trans. Power Electron. vol. 34 (1) (Jan. 2019) 840–848.
[16] M. Zolfaghari, M. Abedi, G.B. Gharehpetian, Power flow control of interconnected AC–DC microgrids in grid-connected hybrid microgrids using modified UIPC, IEEE Trans. Smart Grid vol. 10 (6) (Nov. 2019) 6298–6307.
[17] F. Nejabatkhah, Y.W. Li, Overview of power management strategies of hybrid AC/DC microgrid, IEEE Trans. Power Electron. vol. 30 (12) (Dec. 2015) 7072–7089.
[18] Z. Yi, W. Dong, A.H. Etemadi, A unified control and power management scheme for PV-battery-based hybrid microgrids for both gridconnected and islanded modes, IEEE Trans. Smart Grid vol. 9 (6) (Nov. 2017) 5975–5985.
[19] J.-H. Teng, S.-W. Luan, D.-J. Lee, Y.-Q. Huang, Optimal charging/discharging scheduling of battery storage systems for distribution systems interconnected with sizeable PV generation systems, IEEE Trans. Power Syst. vol. 28 (2) (May 2013) 1425–1433.
[20] B. Papari, C.S. Edrington, I. Bhattacharya, G. Radman, Effective energy management of hybrid AC–DC microgrids with storage devices, IEEE Trans. Smart Grid vol. 10 (1) (Jan. 2019) 193–203.
[21] P.T. Baboli, M. Shahparasti, M.P. Moghaddam, M.R. Haghifam, M. Mohamadian, Energy management and operation modelling of hybrid AC–DC microgrid, IET Gen. Trans. Dist. vol. 8 (10) (Oct. 2014) 1700–1711.
[22] A.A.A. Radwan, Y.A.-R.I. Mohamed, Networked Control and Power Management of AC/DC Hybrid Microgrids (vol. PP), IEEE Sys. J. (99) (October 2014) 1–12.
[23] C. Liu, B. Zhang, Y. Hou, F.F. Wu, Y. Liu, An improved approach for AC-DC power flow calculation with multi-infeed DC systems, IEEE Trans. Power Syst. vol. 26 (2) (May 2011) 862–869.
[24] Y.-S. Tzeng, N. Chen, R.-N. Wu, A detailed R-L fed bridge converter model for power flow studies in industrial AC/DC power systems, IEEE Trans. Ind. Electron. vol. 42 (5) (Oct. 1995) 531–538.
[25] Z.S. Molaee, E. Rokrok, M. Doostizadeh, A unified power flow approach using VSC-efficiency for AC-DC distribution systems operating at grid connected and islanded modes, Int. J. Elect. Power Energy Syst. vol. 130 (2021) 106906 (Art. no).
[26] L. Jia, Y. Zhu, S. Du, Y. Wang, Analysis of the transition between multiple operational modes for hybrid AC/DC microgrids, CSEE J. Power Energy Syst. vol. 4 (1) (2018) 49–57.
[27] J. Rocabert, A. Luna, F. Blaabjerg, P. Rodríguez, Control of power converters in AC microgrids, IEEE Trans. Power Electron. vol. 27 (11) (Nov. 2012) 4734–4749.
[28] S. Peyghami, H. Mokhtari, F. Blaadjerg, Autonomous operation of a hybrid AC/DC microgrid with multiple interlinking converter, IEEE Trans. Smart Grid vol. 9 (6) (Nov. 2018) 6480–6488.
[29] A. Sangwongwanich, Y. Yang, F. Blaabjerg, High-performance constant power generation in grid-connected PV systems, IEEE Trans. Power Electron. vol. 31 (3) (2016) 1822–1825.
[30] A. Sangwongwanich, Y. Yang, F. Blaabjerg, H. Wang, Benchmarking of constant power generation strategies for single-phase gridconnected photovoltaic systems (Jan./Feb), IEEE Trans. Ind. Appl. vol. 54 (1) (2018) 447–457 (Jan./Feb).
[31] J.C. Vasquez, J.M. Guerrero, A. Luna, P. Rodriguez, R. Teodorescu, Adaptive droop control applied to voltage-source inverters operating in grid-connected and islanded modes, IEEE Trans. Ind. Electron. vol. 56 (10) (Oct. 2009) 4088–4096.
[32] S. Moradi, G. Zizzo, S. Favuzza, F. Massaro, A stochastic approach for self-healing capability evaluation in active islanded AC/DC hybrid microgrids, Sustain. Energy, Grids Netw. vol. 33 (Mar. 2023) 100982 (Art. no).
[33] S. Moradi, V. Vahidinasab, G. Zizzo, ‘‘Optimal nanogrid planning at building level,’’, Int. J. Electr. Power Energy Syst. vol. 153 (Nov. 2023) 109409 (Art. no).
[34] https://zenodo.org/communities/hyperride/search?page=2&size=20..
[35] Eurostat, Energy, transport and environment statistic, 2019.
[36] REN 21, Renewables 2019 Global Status Report, REN 21, 2019.
[37] Terna SpA, SNAM documento di descrizione degli scenari 2019, 2019.
[38] IRENA, Global Energy Transformation, a Roadmap to 2050, IRENA, 2018.
[39] IRENA, Electricity Storage and Renewables: Costs and Markets to 2030, IRENA, 2017.